Angewandte Chemie
Eine Zeitschrift der Gesellschaft Deutscher Chemiker

Supporting Information

Saving the Energy Loss in Lithium-Mediated Nitrogen Fixation by Using a Highly Reactive Li_3N Intermediate for C–N Coupling Reactions

G.-F. Chen, A. Savateev, Z. Song, H. Wu, Y. Markushyna, L. Zhang, H. Wang*, M. Antonietti**

Supporting Information

Table of Contents

I. Experimental Methods

Electrolyte preparation:

Electrolyte solutions were prepared by dissolving 1.0 M $LiClO_4$ (Sigma-Aldrich, battery grade, dry,) in PC (Sigma-Aldrich, anhydrous, 99.7%), THF (Sigma-Aldrich, anhydrous, ⩾ 99.9%, inhibitor-free), or their mixture. The clear solution was used directly and transferred to electrolytic cell. The THF with lower water content was obtained by adding approximately 60% v/v of molecular sieves (VWR, 4 Å) to the solvent in a bottle. The bottle was then sealed from the atmosphere with a PTFE cap, and then the THF was kept away from light and dried for 48 hours. The molecular sieves were activated for four hours at 250 ^{o}C in a vacuum dryer before being used for drying.

Electrochemical Li-mediated N_2 reduction:

For Li plating in battery, the two-electrode cells containing Cu foil electrode (1.13 cm^2), separator, electrolyte (180 μL), and lithium foil as counter electrode were assembled in a glove box filled with pure Ar. The electrolytes used in the experiments were standard ester-type electrolyte 1 M $LiPF_6$/ethylene carbonate/diethyl carbonate (EC:DEC=1:1 by volume, from Sigma) and 1 M $LiPF_6$/EC:DEC:EMC=1:1:1 (by volume) with 2 wt% vinylene carbonate (VC) additive (from E-Lyte Innovations GmbH). Large electrolytic cell for lithium plating was separated into two compartments by PE film (16 μm thick). During lithium deposition, a stainless steel mesh substrate (SSM, 1 cm^2), Pt foil (1 cm^2), and Ag/Ag^+ electrode (Ag wire in 0.1 M $AgClO_4$ in THF) were served as cathode, anode, and reference electrode, respectively. For PC//THF+PC system, the cathodic compartment was filled with 12 mL of 1.0 M $LiClO_4$/PC solution, and the anodic compartment was filled with 12 mL of 1.0 M $LiClO_4$/THF+PC (THF:PC=1:1) mixed solution. For comparison, other non-reactive solvents, such as 1,3-dioxolane (DOL) and 1,2-dimethoxyethan (DME) were also used to prepare the mixed electrolyte by replacing THF. For THF//THF system and PC//PC system, the catholyte and anolyte were identical. For lithium plating on SSM, chronopotentiometry was carried out at current density of –15 mA cm^{-2} using a Gamry instrument at room temperature.

Nitridation of Li-deposited electrodes were conducted in a 50 mL round-bottom flask, through which N_2 gas (99.999 %) flows at a rate of 30 mL min^{-1} to ensure N_2 atmosphere within the flask. The flask was located on a heating mantle, whose temperature had already been set to be at a desired temperature level. Li-deposited electrode with the immersion in THF for 10 s was then placed in the flask (The performance comparison with and without the immersion in THF can be seen in Figure S42). The exposure of deposited Li to N_2 atmosphere was carried out at 220 ℃ for 30 min. The performance comparison after nitridation at several temperature levels can be seen in Supplementary Figure S43.

Control experiments were carried out in the aforementioned round-bottom flask using pure argon instead of N_2. Feed gases passed through three solutions before entering the cell to purify and prepare the gas. First, the gases were passed through 0.1 M NaOH to capture any NO_x, then 0.1 M HCl to capture any NH_3, and finally through PC with molecular sieves to capture water in the gaseous stream. For the isotope labeling experiment, 30 mL min^{-1} of argon gas was initially passed through the round-bottom flask to remove air, and then 10 mL min^{-1} of $^{15}N_2$ (Sigma-Aldrich, 98 atom % ^{15}N, 5 L) was fed to the round-bottom flask for nitridation experiment (Detailed discussion in Figures S44, S45).

Detection of produced Li_3N and performance evaluation:

The generated Li_3N was detected and quantified by detecting the ammonia in the solution after the hydrolysis of Li_3N in 100 mL of 0.05 M hydrochloric acid solution. The reaction between the Li_3N and acid was so fast that the surface of current collector instantaneously and completely refreshed. The ammonia in the 0.05 M hydrochloric acid solution was quantified by the indophenol blue method using the spectrophotometric analysis, whose maximum absorbance occurred at a wavelength of 660 nm. The performances in this work are evaluated by Faradaic efficiency and yield rate. The Faradaic efficiency calculations consider both the Li plating and Li nitridation process and the integrated value for the final synthesis of Li_3N product can be calculated as $FE = (nF \times c \times V)/(M \times Q)$, where n is the number of transferred electrons, F is the Faraday constant, c is the measured NH_3 concentration in solution after the hydrolysis of Li_3N, V is the volume of the hydrochloric acid solution for the hydrolysis of Li_3N, M is the relative molecular mass of NH_3 and Q is the total charge used for electroplating. The amount of Li_3N produced at a specific time was calculated using the $m = (c \times V)/M$. Considering the nitride and hydrolysis steps are fast, in this work only the plating time was taken into account in calculating the yield rate.

Synthesis of aryl imides:

A 2 mL glass bottle with a rubber stopper was placed the Li_3N (Sigma-Aldrich ,⩾99.5%) or Li_3N-loaded electrodes in 0.2 mL of THF (Sigma-Aldrich, anhydrous, ⩾99.9%, inhibitor-free). Stirring was started and various equivalents of aryl acid chlorides in 0.3 mL of THF were added over a 30-min period. Stirring was then continued for an additional 6 hours. After reaction, the solution was diluted with 2 mL of hydrochloric acid (1 M) and extracted with ethyl acetate (4 × 2 mL). All organic solutions were combined and evaporated for the GC-MS measurements. To give purified products, the volatiles were evaporated and the resulting crude product was purified by silica gel chromatography (eluent: Hexane/ethyl acetate) or recrystallization. For the method of recrystallization, the organic solution was washed with 10% aqueous H_2SO_4 leading to the formation of a crystalline precipitate, which was collected by filtration. Here, representative aryl acid chlorides include benzoyl chloride (Sigma-Aldrich, 99%), o-phthaloyl chloride (Sigma-Aldrich, 90%), phenylacetyl chloride (Sigma-Aldrich, 98%), p-toluoyl chloride (Sigma-Aldrich, 98%), mixture of benzoyl chloride and p-toluoyl chloride (with mole ratio of 1:2). Some of commercial acid chlorides may contain a lot of carboxylic acid and HCl impurities derived from hydrolysis of acid chlorides. In this case, the Li_3N will react with HCl instead of acid chloride. In this work, phenylacetyl chloride and p-toluoyl chloride were gone through a 24-hour treatment by molecular sieve for adsorption of impurities before using for the reactions to enhance the selectivity for the synthesis of aryl imides. The yield and FE were calculated based on amount of objective product quantified by the GC-MS.

Physicochemical characterization:

The chemical groups of SEI were tested by Fourier transform infrared spectroscopy (Bruker VERTEX 33). XRD measurements were performed on a Bruker D8 Advance diffractometer equipped with a scintillation counter detector with CuKα radiation (λ = 0.15418 nm) applying a 2θ angle in the range 5–80 °. The surface morphology and structure of the prepared samples were analysed by field emission scanning electron microscopy (FESEM, Regulus SU8100) and TEM (300 kV; Tecnai G2 F30). The surface valence and chemical bonds of the samples were tested by X-ray photoelectron spectroscopy on an ESCALAB 250 spectrometer (Thermo Fisher Scientific) with monochromatic Al Kα radiation (1486.6 eV). ^{1}H and ^{13}C NMR spectra were recorded on Agilent 400 MHz. Mass spectral data were obtained using Agilent GC 6890 gas chromatograph, equipped with HP5MS column (inner diameter = 0.25 mm, length = 30 m,

and film= 0.25 μm), coupled with Agilent MSD 5975 mass spectrometer (electron ionization). Water content analysis in THF or PC was carried out by the Karl Fischer titration method.

DFT calculations:

The energic, structural, and electronic (electron density) performances have been calculated using DMol^3 code.[1,2] The generalized gradient approximation (GGA) with the Perdew–Burke–Ernzerhof (PBE) functional[3] and all-electron double numerical basis set with polarized function (DNP) have been employed. The convergence tolerance of energy, maximum force and maximum displacement are 1.0 $\times 10^{-5}$ Ha, 2.0 $\times 10^{-3}$ Ha/Å and 5.0 $\times 10^{-3}$ Å (1Ha = 627.51 Kcal mol^{-1}) for geometry optimization. The Grimme method for DFT-D correction is considered for all calculations.[4] Each atom in the storage models is allowed to relax to the minimum in the enthalpy without any constraints. The reactants and products were built, then the energy of all systems was calculated.

The free energy change (ΔG) of each reaction step is estimated by the equation[5]:

$$\Delta G = \Delta E + \Delta E_{ZPE} - T\Delta S \qquad (1)$$

where ΔE is the adsorption energy by DFT calculation, ΔE_{ZPE} and ΔS denote the changes of zero-point energy and entropy. The temperature T is set to 300 K.

Reaction energy ΔE of was defined as:

$$\Delta E = E_{(C6CON)3} + 3{*}E_{HCl\ or\ LiCl} - (E_{C6COCl} + E_{NH3\ or\ Li3N}) \qquad (2)$$

where *A and * denotes the adsorption of A group on substrates and the bare substrates, E_A denotes the energy of A group.

Synthesis of aryl imides via the amidation reaction of the benzamide 1 by benzoyl chloride:

N-benzoylbenzamide **2** was prepared following previous literature study.[6] Benzamide (1.0 g, 8.3 mmol) was dissolved in pyridine (15 mL) and cooled to 0 ℃. After the dropwise addition of benzoyl chloride (1.2 mL, 8.3 mmol) the reaction mixture was stirred at 0 ℃ for 8 h, then H_2O (15 mL) was added in one portion to the reaction. The reaction mixture was extracted with Et_2O (2 × 15 mL). The organic phases was washed with 10% aqueous H_2SO_4 leading to the formation of a colorless crystalline precipitate, which was collected by filtration. A second crop of crystals can be obtained from the organic layer upon standing. The combined precipitate was recrystallized from EtOAc to afford N-benzoylbenzamide **2** as colorless needles.

N-benzoylbenzamide 2a

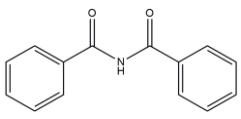

Yield: 9%. ^{1}H NMR (400 MHz, DMSO-d_6) δ 11.32 (s, 1H), 7.91-7.88 (m, 4H), 7.64-7.60 (m, 2H), 7.52-7.48 (m, 4H). ^{13}C NMR (400 MHz, DMSO-d_6) δ 168.15, 134.26, 133.08, 129.09, 128.84.

Synthesis of aryl imides via the acylation reaction of the Li_3N by benzoyl chloride:

A 2 mL glass bottle with a rubber stopper was placed the Li_3N (Sigma-Aldrich, ⩾99.5%) in 0.2 mL of THF (Sigma-Aldrich, anhydrous, ⩾99.9%, inhibitor-free). Stirring was started and various equivalents of aryl acid chlorides in 0.3 mL of THF were added over a 30-min period. Stirring was then continued for an additional 6 hours. After reaction, the solution was diluted with 2 mL of hydrochloric acid (1 M) and extracted with ethyl acetate (4 ×2 mL). All organic solutions were combined and evaporated for the GC-MS measurements. To give purified products, the volatiles were evaporated and the resulting crude product was purified by silica gel chromatography (eluent: Hexane/ethyl acetate).

N-benzoylbenzamide 2a

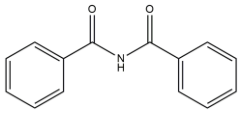

Yield: 88%. ^{1}H NMR (400 MHz, THF-d_8) δ 10.30 (s, 1H), 7.89-7.86 (m, 4H), 7.56-7.52 (m, 2H), 7.46-7.42 (m, 4H). ^{13}C NMR (400 MHz, THF-d_8) δ 167.46, 134.56, 131.94, 128.38, 128.01. ^{1}H NMR (400 MHz, DMSO-d_6) δ 11.35 (s, 1H), 7.92-7.89 (m, 4H), 7.65-7.61 (m, 2H), 7.54-7.50 (m, 4H). ^{13}C NMR (400 MHz, DMSO-d_6) δ 168.18, 134.26, 133.10, 129.11, 128.86.

II. Supporting Figures

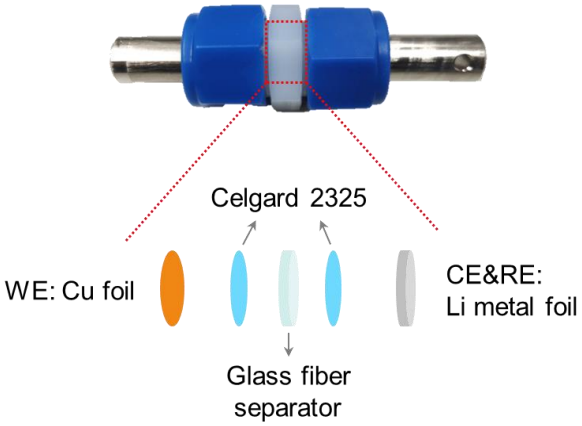

Figure S1. Configuration of assembling battery.

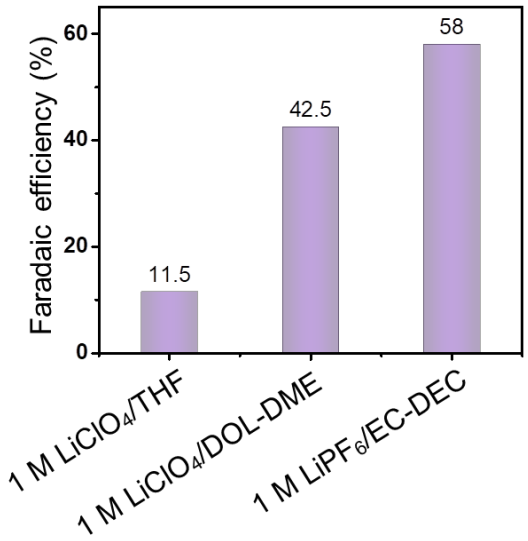

Figure S2. Faradaic efficiencies of the Li_3N synthesis in battery system at current of –5.0 mA using different solvent for electrolyte preparation.

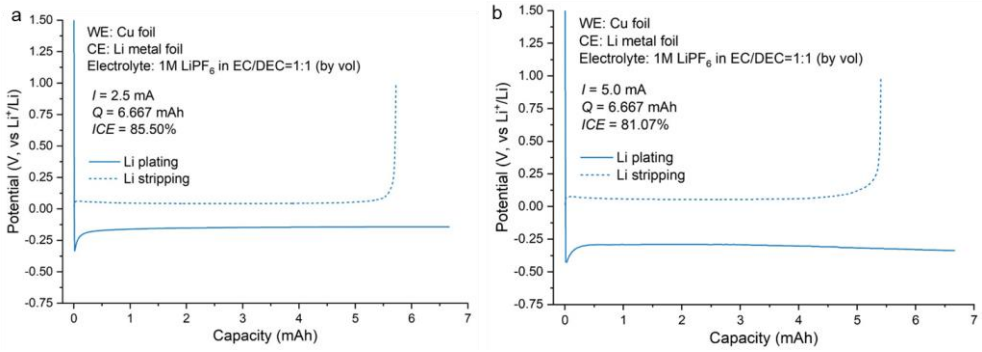

Figure S3. Coulombic efficiency using electrolyte of 1 M $LiPF_6$/EC:DEC=1:1 by volume at current of (**a**) –2.5 mA and (**b**) –5.0 mA.

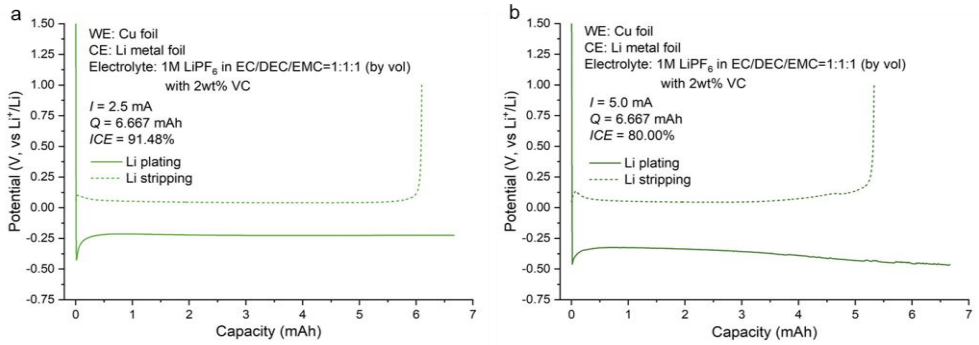

Figure S4. Coulombic efficiency using electrolyte of 1 M $LiPF_6$/EC:DEC:EMC=1:1:1 by volume with 2 wt% VC additive at current of (**a**) –2.5 mA and (**b**) –5.0 mA.

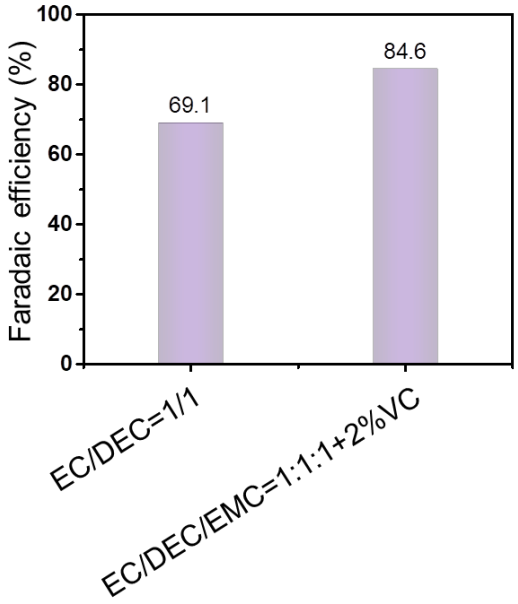

Figure S5. Faradaic efficiencies of the Li_3N synthesis in battery system at current of –2.5 mA using electrolyte of 1 M $LiPF_6$/EC:DEC=1:1 by volume and 1 M $LiPF_6$/EC:DEC:EMC=1:1:1 by vol with 2 wt% VC additive.

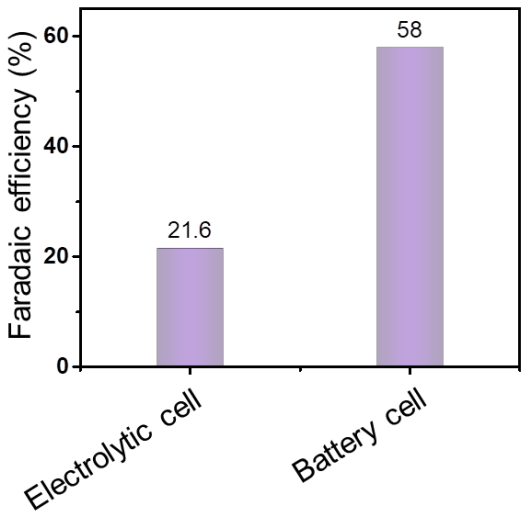

Figure S6. Faradaic efficiencies of the Li_3N synthesis using electrolyte of 1 M $LiPF_6$/EC:DEC=1:1 by volume in large electrolytic cell and battery system at current of –15.0 mA and –5.0 mA, respectively.

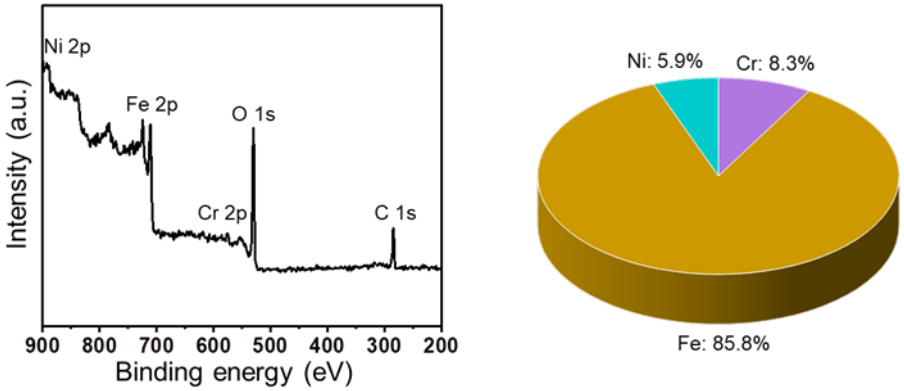

Figure S7. (a) XPS survey spectrum of SSM substrate. (**b)** Corresponding atomic ratio of Fe, Ni, and Cr elements in the SSM substrate.

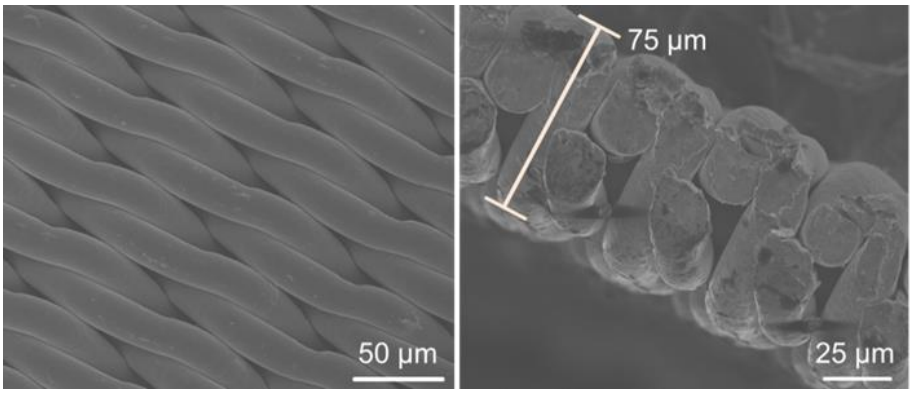

Figure S8. SEM images of the SSM substrate (left: top view; right: side view).

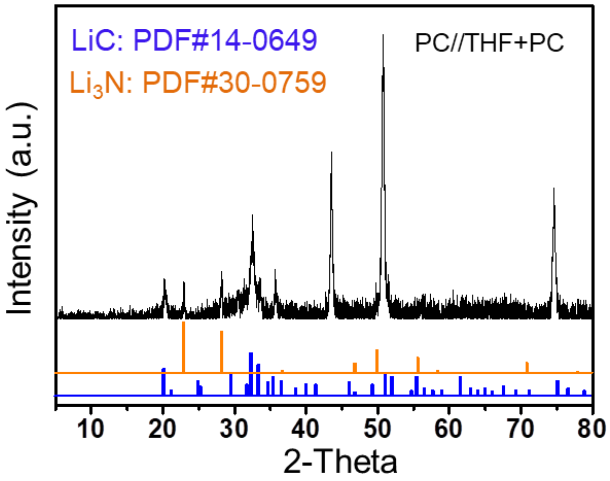

Figure S9. XRD pattern of the Li-deposited SSM electrodes (PC/THF+PC system) after the nitridation process. The Li_3N belongs to the hexagonal P6/mmm(191) space group and is a layered structure composed of sequential Li_2N layers interconnected through Li atoms.

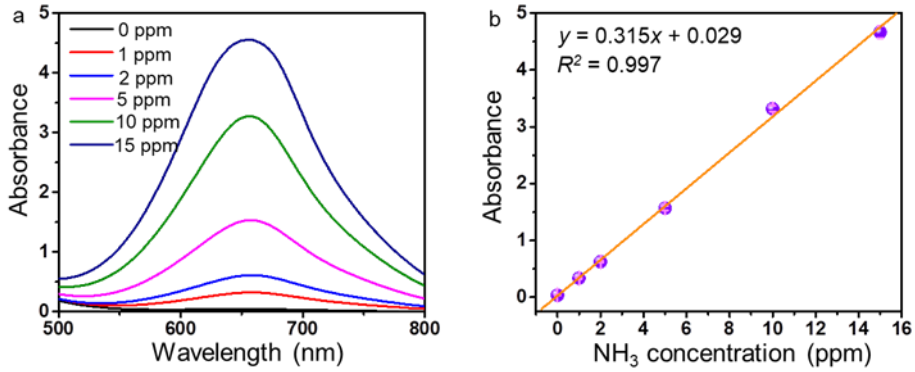

Figure S10. (**a**) UV-vis absorption spectra of solution prepared by mixing the 2 mL of defined amount of NH_3 in 0.05 M hydrochloric acid with 2 ml of a 1 M NaOH solution that contained salicylic acid and sodium citrate, 1 ml of 0.05 M NaClO, and 0.2 ml of 1 wt% $C_5FeN_6Na_2O$. (**b**) Calibration curve using the data from the panel (**a**). The ammonia was quantified by the indophenol blue method using the spectrophotometric analysis, whose maximum absorbance occurred at 660 nm. Error bars denote the standard deviation of absorbance from three independent measurements.

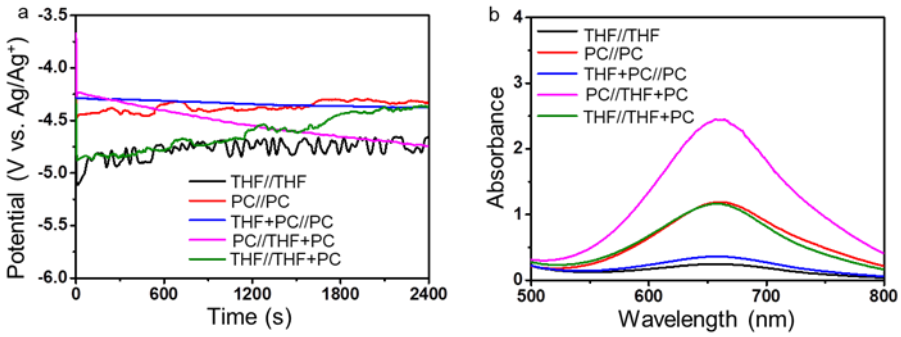

Figure S11. (**a**) Chronoamperometry curves for Li plating in different electrolyte systems with a current density of –15 mA cm^{-2}. (**b**) Corresponding UV-visible absorption spectra for NH_3 measurement after the nitridation and hydrolysis processes.

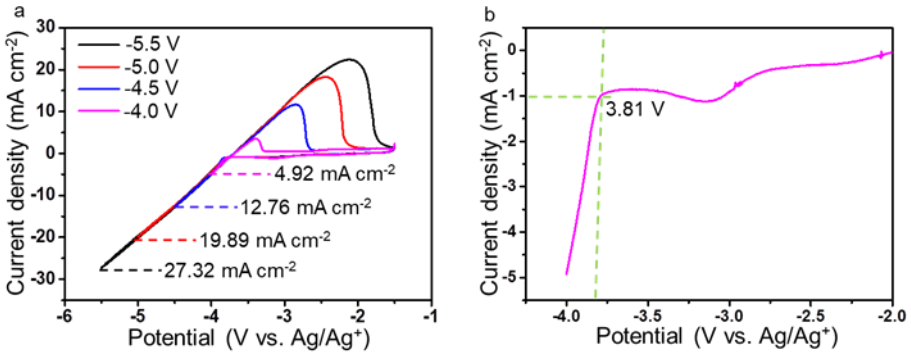

Figure S12. (a) Cyclic voltammograms (CV) under various potentials range in PC//THF+PC system, collected at a sweep rate of 10 mV/s with an Ag/Ag^+ reference. (**b**) Significant current is observed at –3.8 V vs. Ag/Ag^+, which can be attributed to Li^+ reduction reaction in the system. Before Li begins to plate, a reduction peak at ~–3.2 V vs. Ag/Ag^+ due to the formation of SEI is observed.[7,8] The current density of –15 mA cm^{-2} was chosen in order to keep the potential of the working electrode between –4 and –5 V (versus Ag/Ag^+), which can ensure a Coulomb efficiency of more than 60% according to the results of cyclic voltammetry measurements (Figure S13).

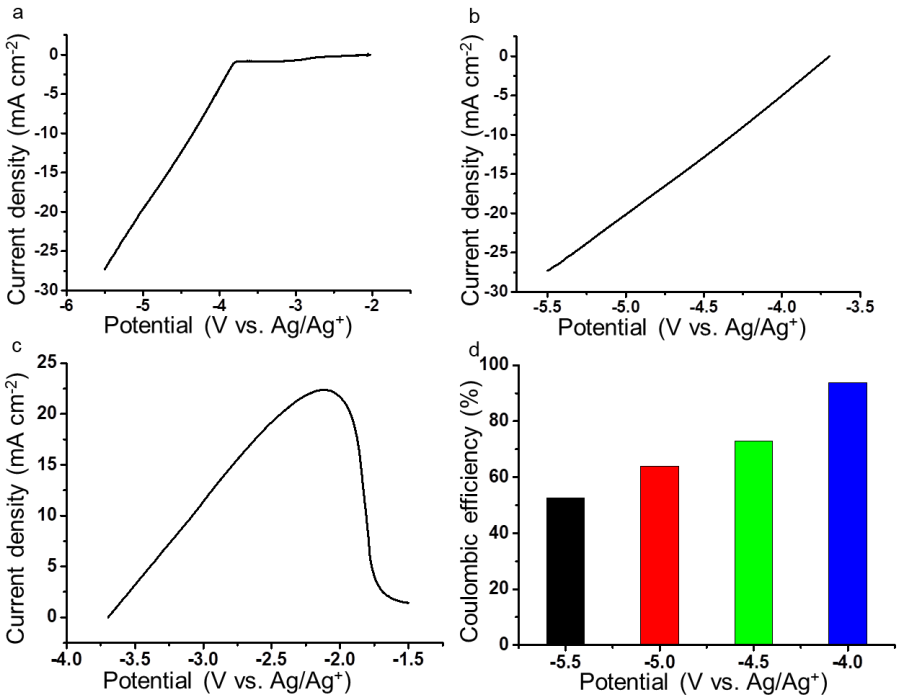

Figure S13. CV curves of (**a**, **b**) for reduction current and (**c**) oxidation current. d, Coulombic efficiency calculated from CV curves.

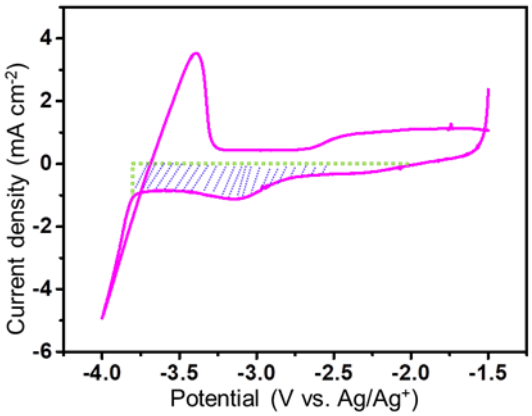

Figure S14. CV curve with a mark of current losses for side reactions before initial Li plating, such as the reduction of PC for the SEI formation.

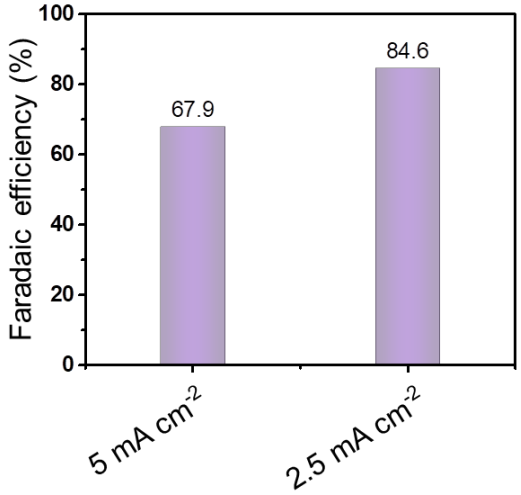

Figure S15. Faradaic efficiencies of the Li_3N synthesis in battery system using electrolyte of 1 M $LiPF_6$/EC:DEC:EMC=1:1:1 by volume with 2 wt% VC additive at current of –2.5 mA and –5.0 mA.

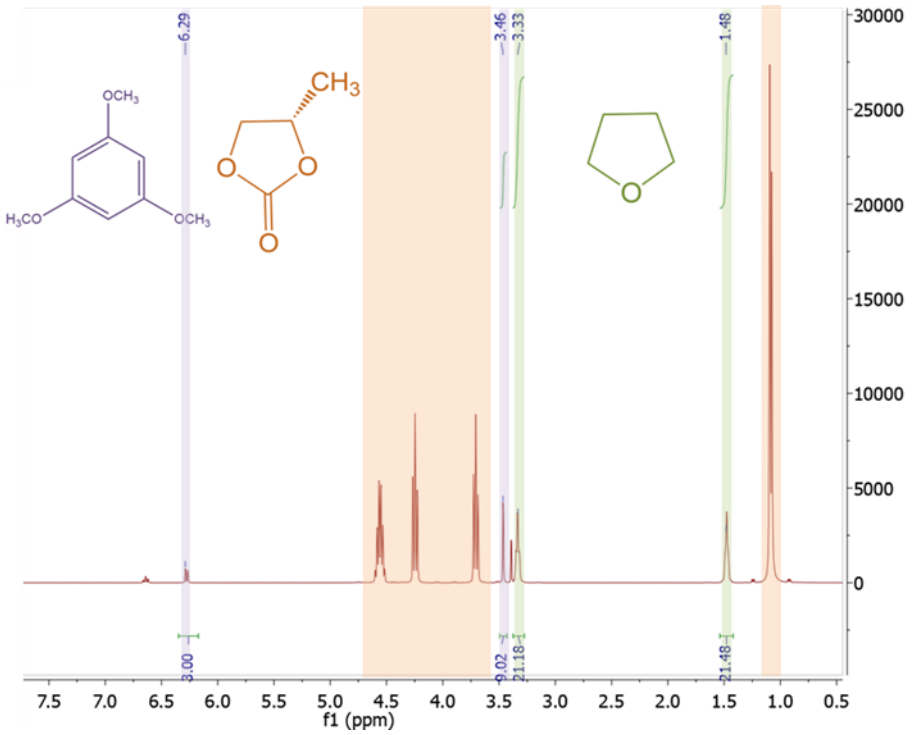

Figure S16. ^{1}H NMR spectra of catholyte from PC//THF+PC system after the electrolyte was sitting in the cell for 40 minutes. The THF permeated from the anolyte to the catholyte and was quantified. 1,3,5-trimethoxybenzene was used as the internal standard. The spectra were collected in DMSO-d_6. Before running enabling the Li plating process, the electrolyte was left sitting in the cell for 40 minutes to allow an initial amount of THF (10.9 mmol) to diffuse from the anolyte to the catholyte.

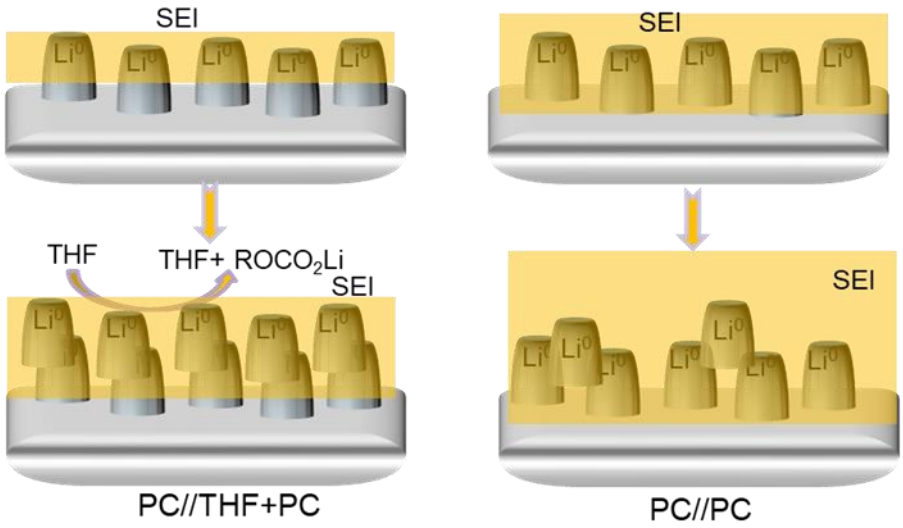

Figure S17. Schematic depiction of Li plating accompanied by the formation of SEI. It shows that, unlike to PC//PC system, right amount of SEI is formed in PC//THF+PC electrolyte because THF here can suppress excessive formation of the thick SEI.

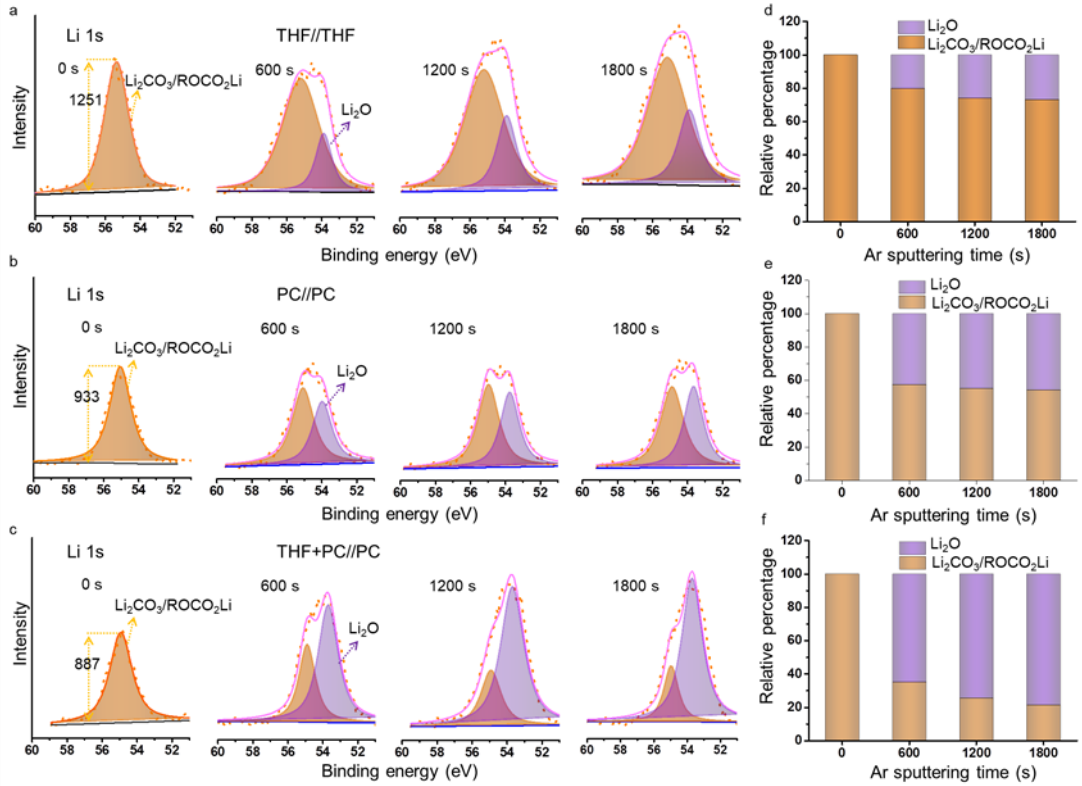

Figure S18. Li 1s XPS conducted on SSM electrodes after plating in (**a**) THF//THF, (**b**) PC//PC, and (**c**) PC/THF+PC systems with various Ar^+-sputtering intervals. The peak area of different compositions with the various etching durations integrating from peak signals of SSM electrodes after plating in (**d**) THF//THF, (**e**) PC//PC, and (**f**) PC/THF+PC systems. They show the abundance of $Li_2CO_3/ROCO_2Li$ species[9] decrease and Li_2O increases for electrodes plating in PC//THF+PC systems compared that in PC//PC system, indicated a less SEI formation but a more active Li plating.

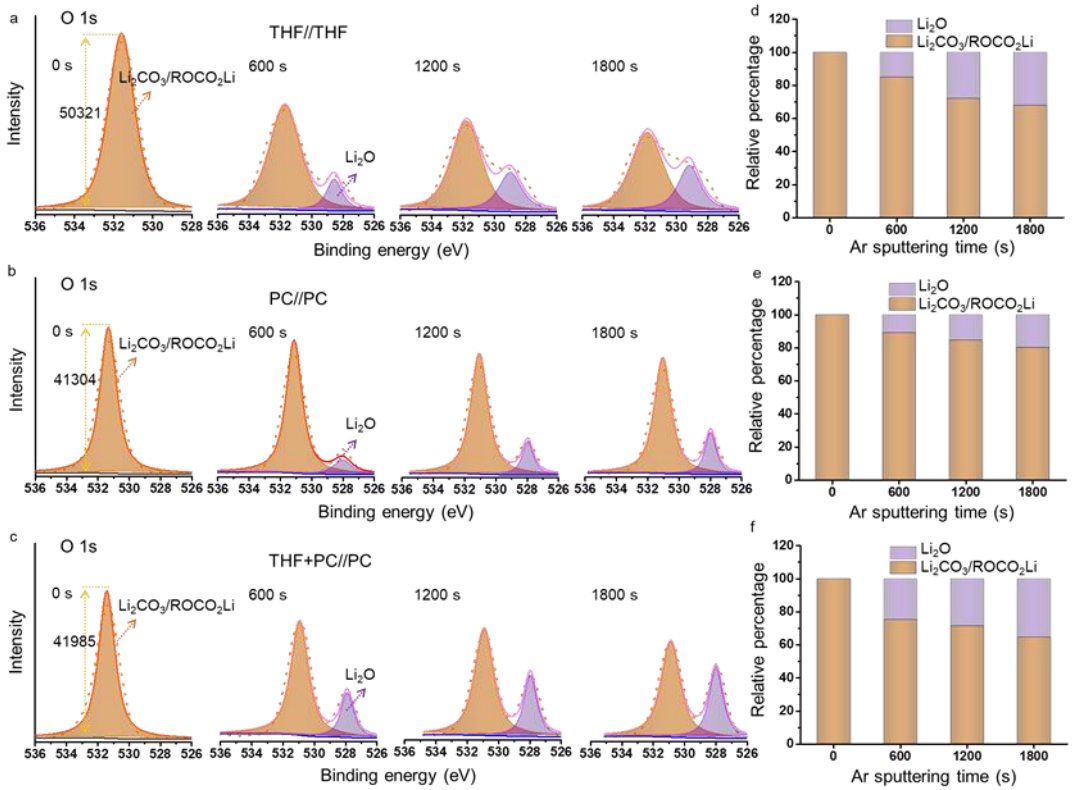

Figure S19. O 1s XPS conducted on SSM electrodes after plating in (**a**) THF//THF, (**b**) PC//PC, and (**c**) PC/THF+PC systems with various Ar^+-sputtering intervals. The peak area of different compositions with the various etching durations integrating from peak signals of SSM electrodes after plating Li in (**d**) THF//THF, (**e**) PC//PC, and (**f**) PC/THF+PC systems. They show the abundance of Li_2CO_3/$ROCO_2Li$ species[9] decrease and Li_2O increases for electrodes plating in PC//THF+PC systems compared that in PC//PC system, indicated a less SEI formation but a more active Li plating.

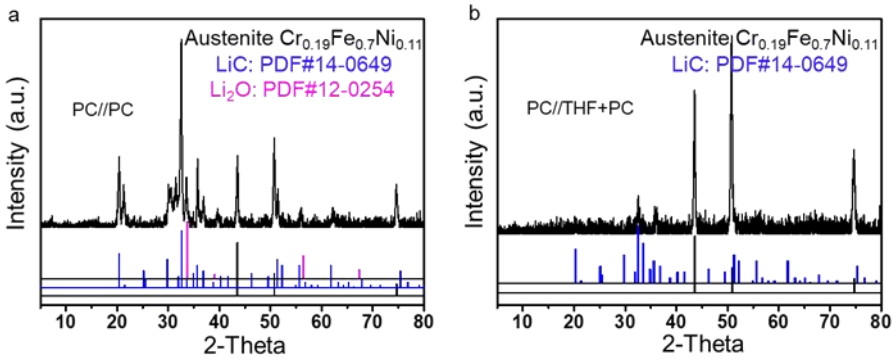

Figure S20. XRD patterns acquired using the SSM electrodes after plating in (**a**) PC//PC, and (**b**) PC/THF+PC systems.

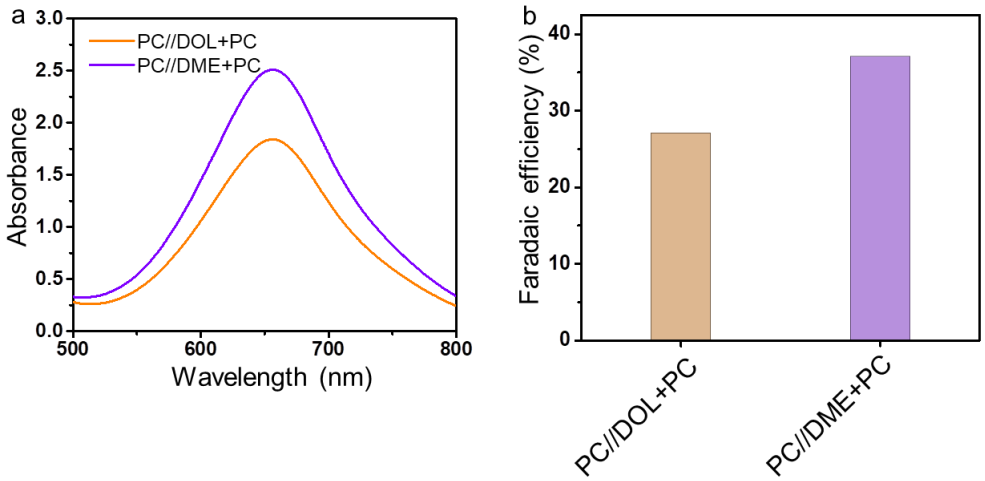

Figure S21. Li_3N synthetic experiments conducted electroplating in PC//DOL+PC and PC//DME+PC system at a current density of –15 mA cm^{-2} for 40 min. (**a**) UV-visible absorption spectra for NH_3 measurement after the nitridation and hydrolysis processes. (**b**) Corresponding Faradaic efficiencies.

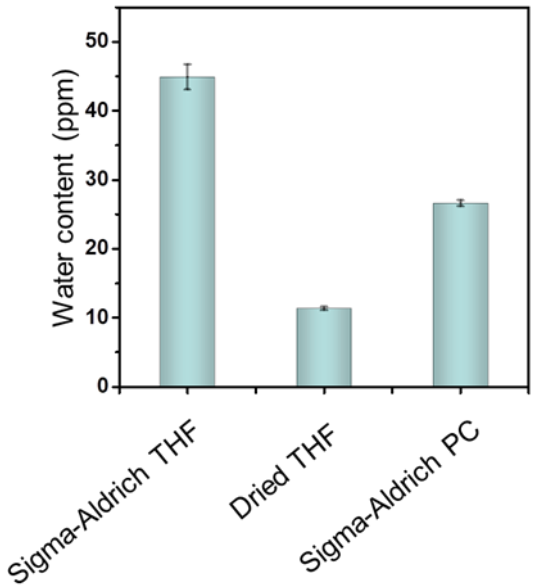

Figure S22. Water content in different solvents determined by the Karl Fischer titration method. The THF desiccated over molecular sieve is denoted as dried THF.

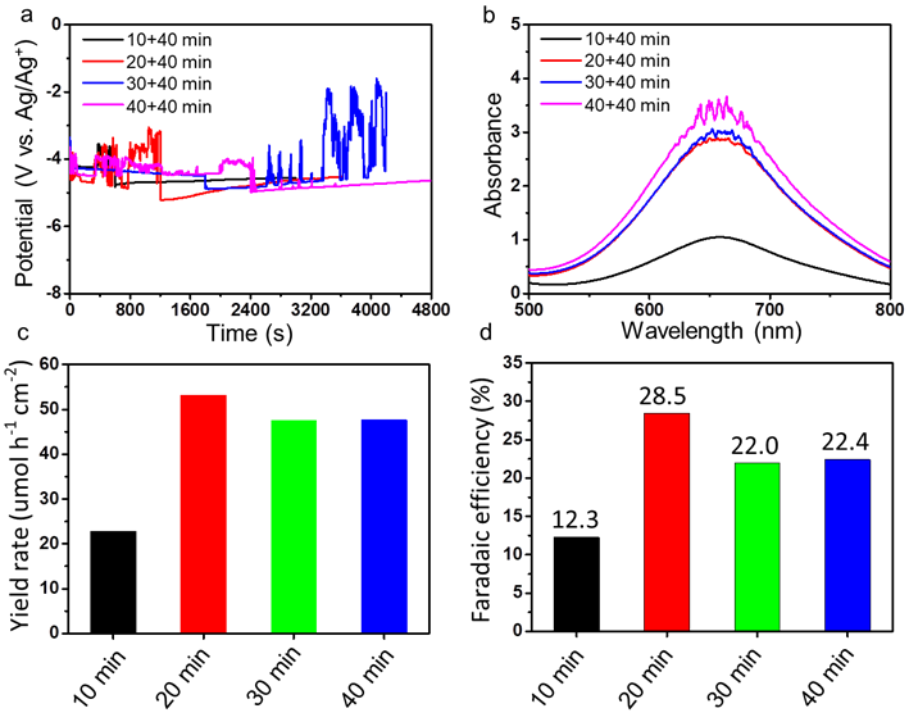

Figure S23. Li_3N synthetic experiments conducted electroplating in PC//THF+PC system for various times to form SEI layer, and then electroplating in THF//THF+PC system with 40 min (all were conducted at a current density of –15 mA cm^{-2}). (**a**) Chronoamperometry curves. (**b**) Corresponding UV-visible absorption spectra for NH_3 measurement after the nitridation and hydrolysis processes. Corresponding (**c**) yield rates and (**d**) the Faradaic efficiencies of Li_3N.

We have studied the effect of Li platting time in PC//THF+PC system ranging from 10 to 40 min, while fixing the time of plating in THF//THF+PC system at 40 min on the FE of Li_3N production (Figure S24). Thus, the optimum FE of 28.5% was obtained for 20 min plating time in PC//THF+PC system followed by plating in THF//THF+PC for 40 min.

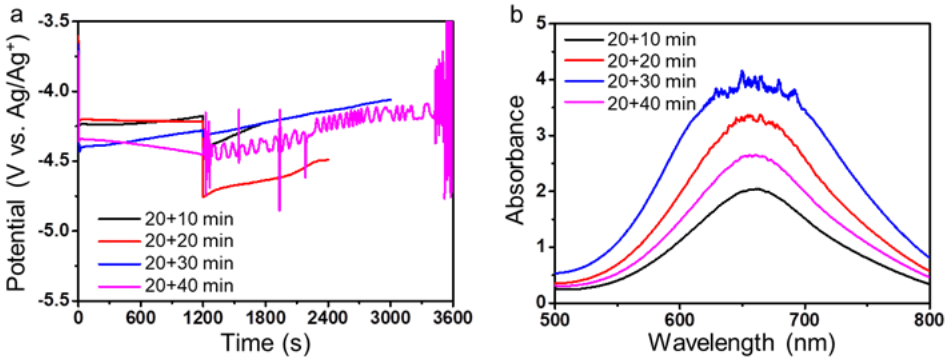

Figure S24. Li_3N synthetic experiments conducted electroplating in PC//THF+PC system for 20 min to form SEI layer, and then electroplating in THF//THF+PC system with various times (all were conducted at a current density of –15 mA cm^{-2}). (**a**) Chronoamperometry curves. (**b**) Corresponding UV-visible absorption spectra for NH_3 measurement after the nitridation and hydrolysis processes.

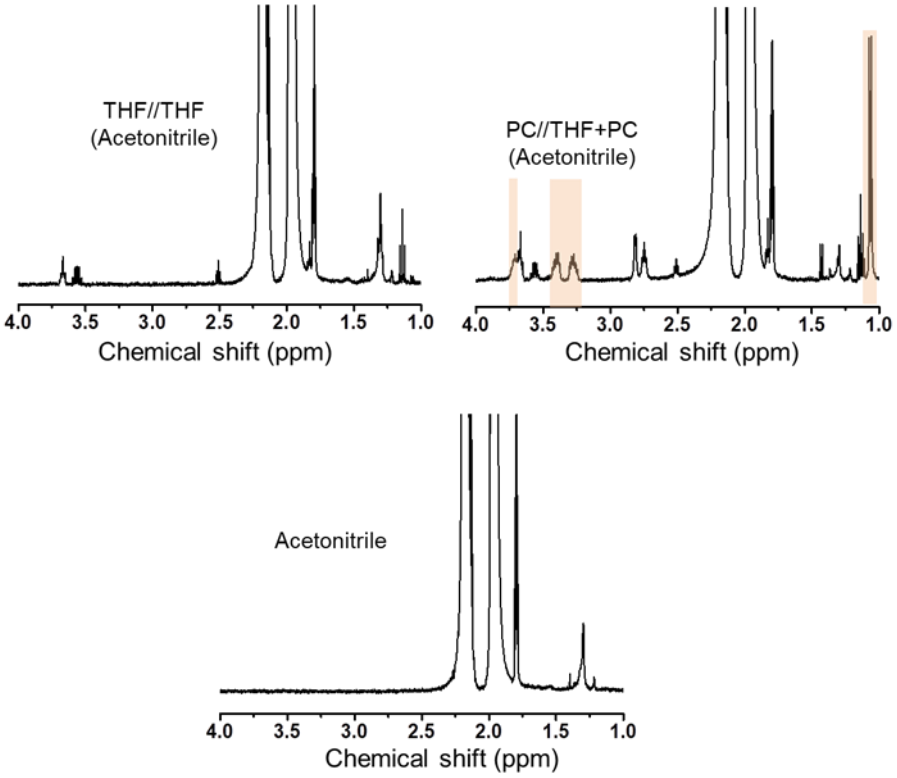

Figure S25. ^1H NMR spectra of the SEI layer acquired after removal form the electrode and dissolution if acetonitrile-d_3. The data shown in the panel (**a**) is for the SEI layer obtained upon Li plating in the THF//THF system and in the panel (**b**) in PC//THF+PC system. (**c**) ^1H NMR spectrum of pure acetonitrile-d_3. The signals marked by yellow rectangles represent the SEI layer derived from PC.

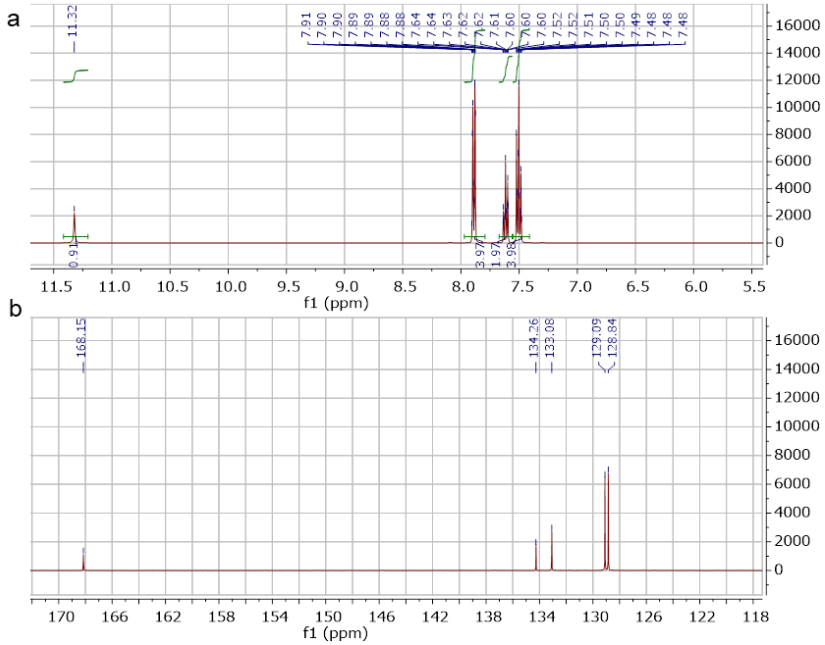

Figure S26. (**a**) ^{1}H and (**b**) ^{13}C NMR spectra of **2a** N-benzoylbenzamide synthesized via the amidation reaction of the benzamide **1** by benzoyl chloride in pyridine solvent. The spectra were collected in DMSO-d_6.

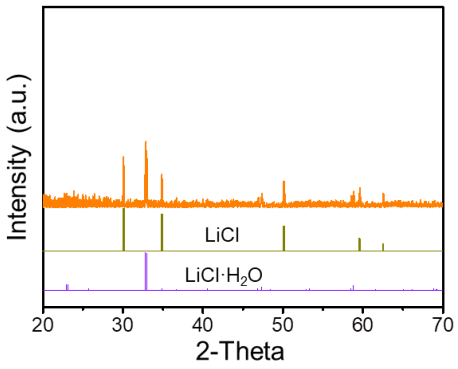

Figure S27. XRD pattern of the collected LiCl after synthetic reaction. The LiCl was separated after imide synthesis by simple extraction and drying. Specifically, after H_2O or diluted HCl was added in reaction solution, the product was extracted with Et_2O. Then LiCl was presented in water phase and the solution was vacuum dried at 200 ^{o}C, washed by diluted HCl, and centrifuged to remove precipitates. And the aboved procedure was repeated for two times. Finally, the obtained white solid was measured by the XRD pattern, showing a pure LiCl crystal with some of LiCl·H_2O. The LiCl·H_2O appears because LiCl absorbed moisture from the air when exposed to the environment during XRD measurement. The recovery rate of lithium is calculated to be 95.4% by measuring the mass of LiCl (10.06 mg) inside the Ar glove box to avoid the hydrolysis of LiCl. The LiCl then can be looped into the formation of Li_3N again.

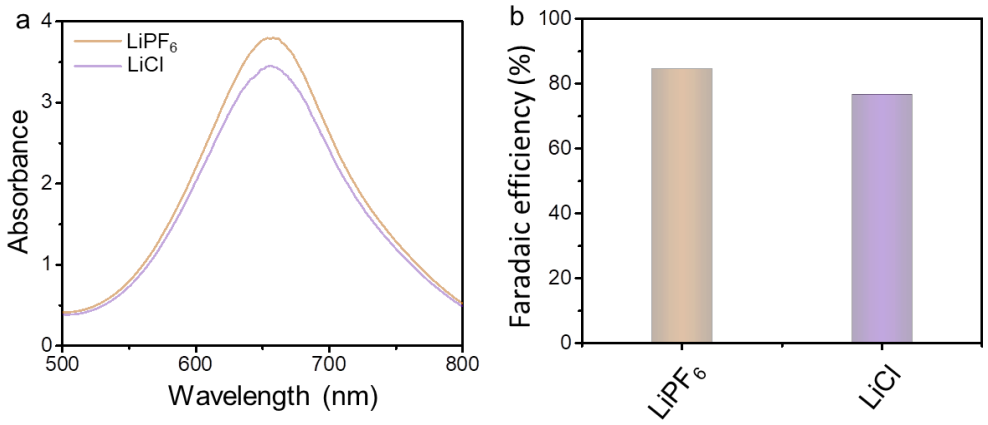

Figure S28. Li_3N synthetic experiments in battery conducted electroplating in 1 M $LiPF_6$/EC:DEC:EMC=1:1:1 by volume with 2 wt% VC additive at current of –2.5 mA for 160 min and 0.2 M LiCl/THF+PC=1:1 by volume at current of –0.5 mA for 800 min. (a) UV-visible absorption spectra for NH_3 measurement after the nitridation and hydrolysis processes. (b) Corresponding Faradaic efficiencies. A high Faradaic efficiency of 76.7% also can be achieved, which is close to that (84.6%) in $LiPF_6$-based electrolyte. The results mean the feasibility of closed cycle of lithium.

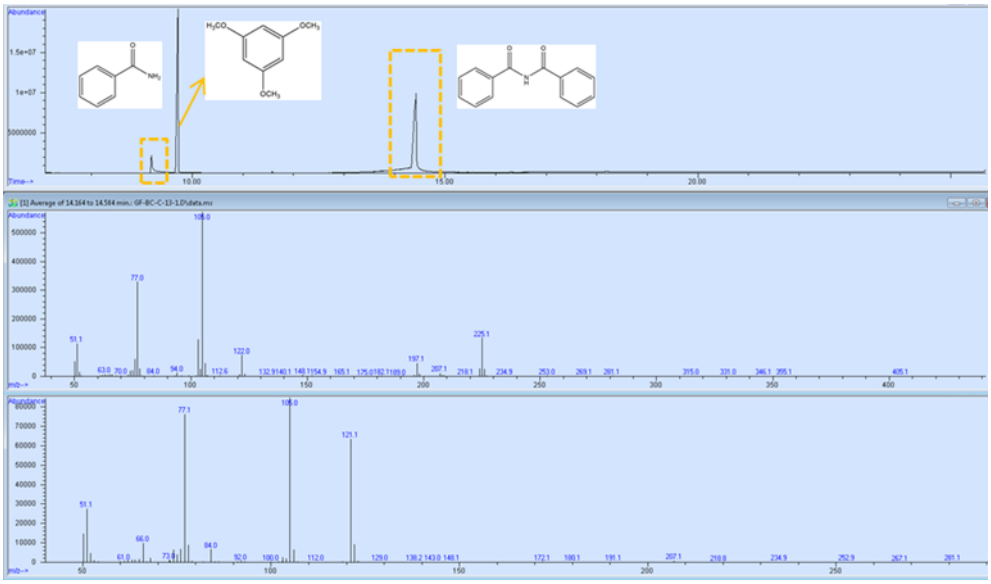

Figure S29. GC-MS data for the reaction mixture solution obtained by mixing Li_3N (0.06 mmol) with one equivalent of benzoyl chloride (0.06 mmol). Theoretical m/z of **2a** N-benzoylbenzamide: 225.1; experimental m/z of **2a** N-benzoylbenzamide: 225.1. Theoretical m/z of **1a** benzamide: 121.1; experimental m/z of **1a** benzamide: 121.1.

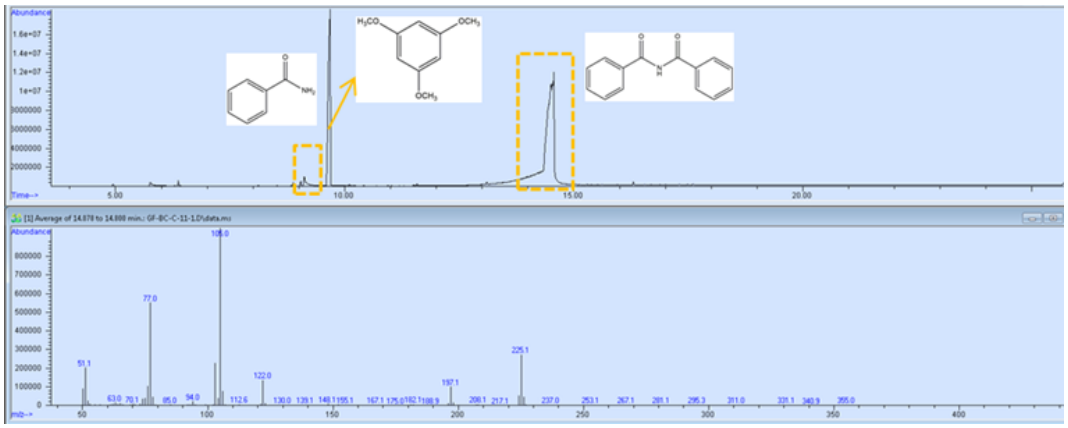

Figure S30. GC-MS data for the reaction mixture solution obtained by mixing Li_3N (0.06 mmol) with two equivalents of benzoyl chloride (0.12 mmol). Theoretical m/z of **2a** N-benzoylbenzamide: 225.1; experimental m/z of **2a** N-benzoylbenzamide: 225.1.

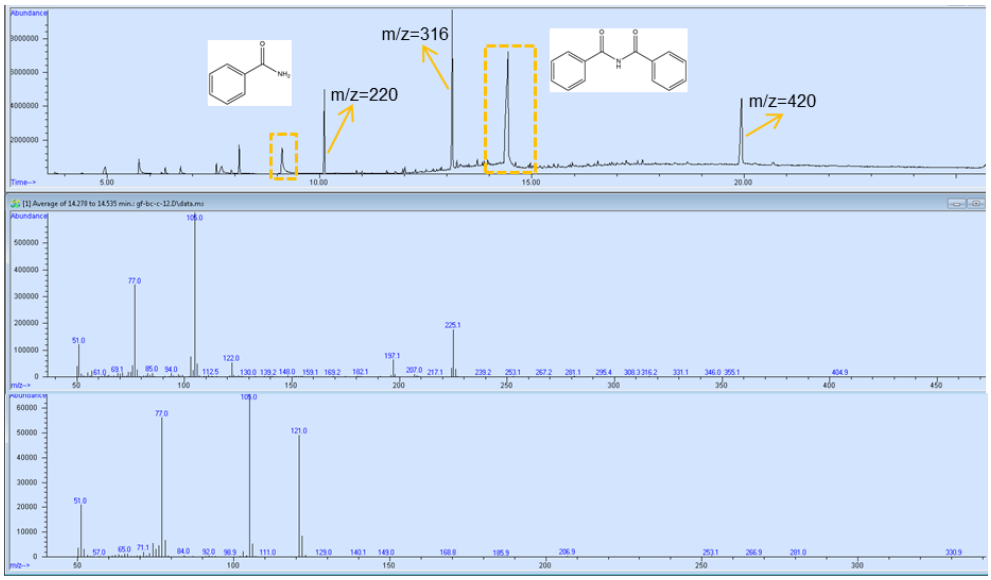

Figure S31. GC-MS data of reaction mixture solution obtained by mixing Li_3N (0.06 mmol) with three equivalents of benzoyl chloride (0.18 mmol). Theoretical m/z of **2a** N-benzoylbenzamide: 225.1; experimental m/z of **2a** N-benzoylbenzamide: 225.1. Theoretical m/z of **1a** benzamide: 121.1; experimental m/z of **1a** benzamide: 121.0.

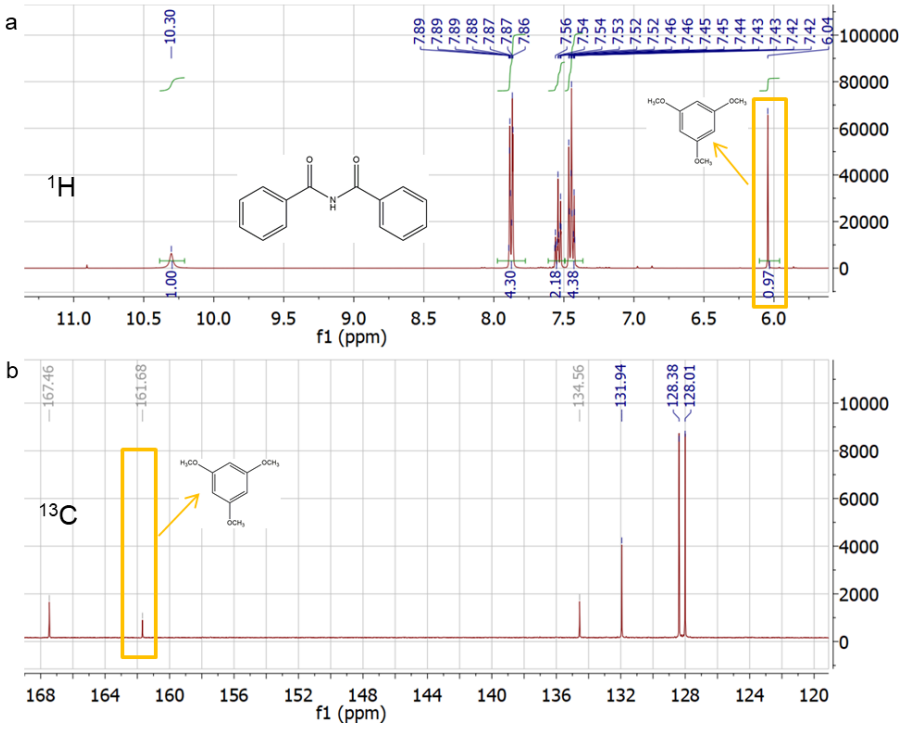

Figure S32. (a) ^{1}H and (**b**) ^{13}C NMR spectra of **2a** N-benzoylbenzamide synthesized via the reaction of Li_3N (0.06 mmol) with two equivalent of benzoyl chloride (0.12 mmol). The spectra were collected in THF-d_8 with 1,3,5-trimethoxylbenzene as the internal standard (^{1}H NMR δ 6.04 (s, 3H); ^{13}C NMR δ 161.68).

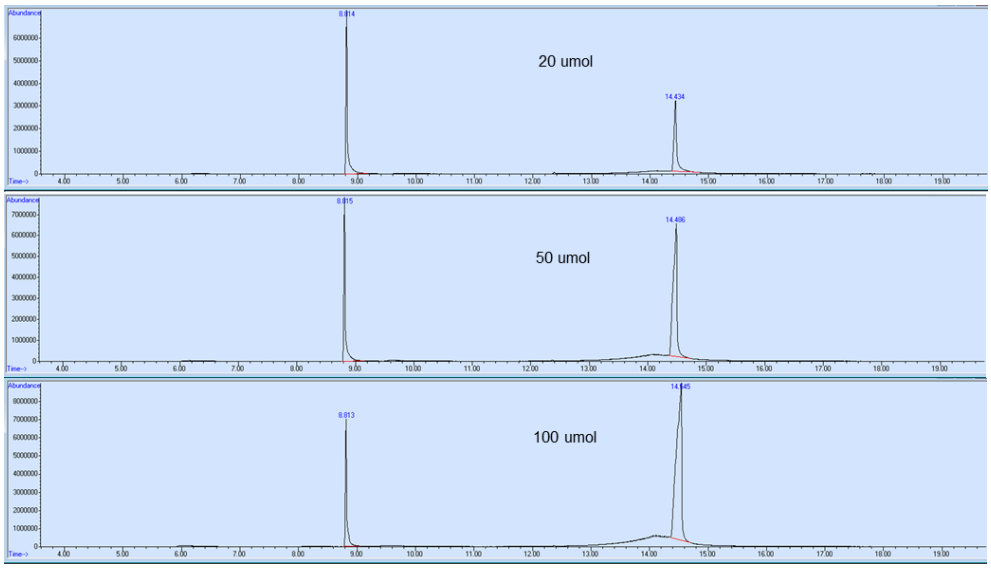

Figure S33. GC-MS data of N-benzoylbenzamide with different amount. Calibration curve ($y = 0.23x - 1.00$, $R^2 = 98.8\%$) can be drawn taking the amount of N-benzoylbenzamide as the X-axis (μmol), the its ratio of integral peak area relative to single ion (m/z = 168.1) signal peak of internal standard (1,3,5-trimethoxybenzene) as the Y-axis.

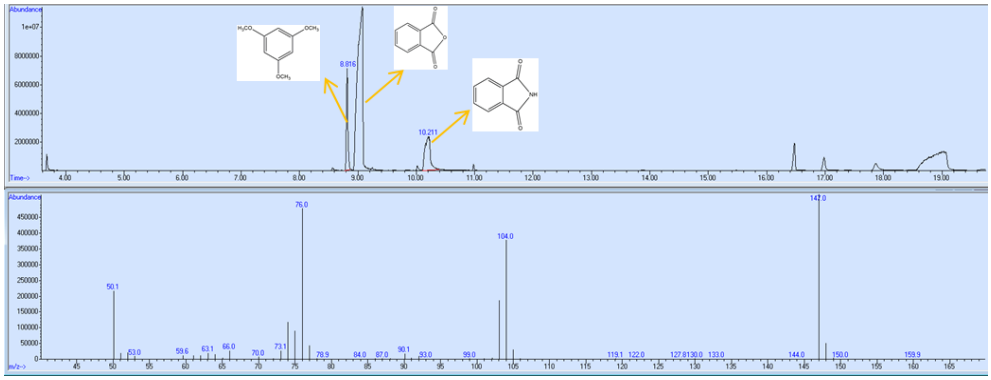

Figure S34. GC-MS data of reaction solution for the Li_3N (0.045 mmol) reacts with o-phthaloyl chloride (0.12 mmol). Theoretical m/z of isoindoline-1,3-dione: 147.0; experimental m/z of isoindoline-1,3-dione: 147.0. The yield is calculated as 91% based on the amount (41 μmol) of isoindoline-1,3-dione calculated from its ratio of integral peak area relative to signal peak of internal standard (1,3,5-trimethoxybenzene) in the GC-MS chromatogram.

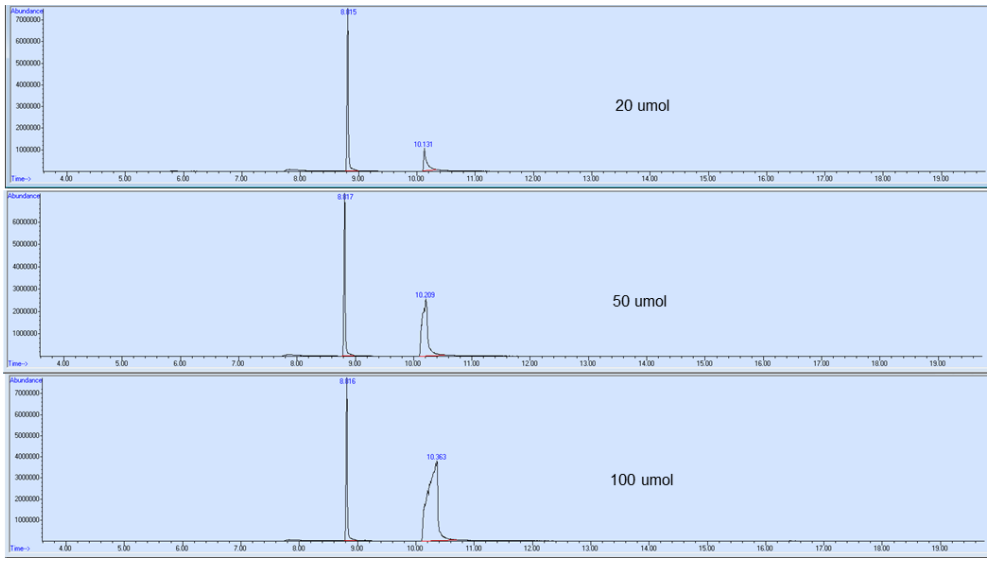

Figure S35. GC-MS data of isoindoline-1,3-dione with different amount. Calibration curve (y = 0.034x – 0.218, R^2 = 97.5%) can be drawn taking the amount of isoindoline-1,3-dione as the X-axis (μmol), the its ratio of integral peak area relative to signal peak of internal standard (1,3,5-trimethoxybenzene) as the Y-axis.

Figure S36. GC-MS data of reaction solution for the (0.045 mmol) reacts with phenylacetyl chloride (0.18 mmol) after drying treatment of molecular sieve for 24 hours. Theoretical m/z of 2-phenyl-N-(2-phenylacetyl)acetamide: 253.1; experimental m/z of 2-phenyl-N-(2-phenylacetyl)acetamide: 253.1. The yield is calculated as 72% based on the amount (33 μmol) of 2-phenyl-N-(2-phenylacetyl)acetamide calculated from its ratio of integral peak area relative to signal peak of internal standard (N-benzoylbenzamide) in the GC-MS chromatogram.

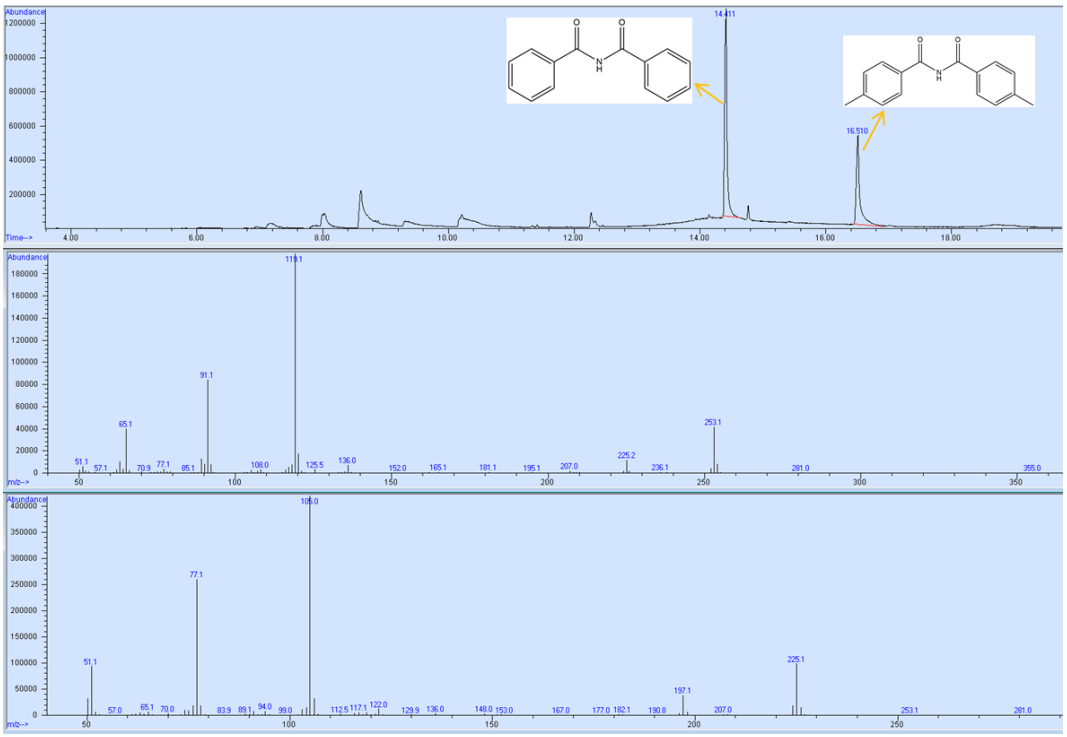

Figure S37. GC-MS data of reaction solution for the (0.045 mmol) reacts with p-toluoyl chloride (0.18 mmol) after drying treatment of molecular sieve for 24 hours. Theoretical m/z of 4-methyl-N-(4-methylbenzoyl)benzamide: 253.1; experimental m/z of 4-methyl-N-(4-methylbenzoyl)benzamide: 253.1. The yield is calculated as 69% based on the amount (31 μmol) of 4-methyl-N-(4-methylbenzoyl)benzamide calculated from its ratio of integral peak area relative to signal peak of internal standard (N-benzoylbenzamide) in the GC-MS chromatogram.

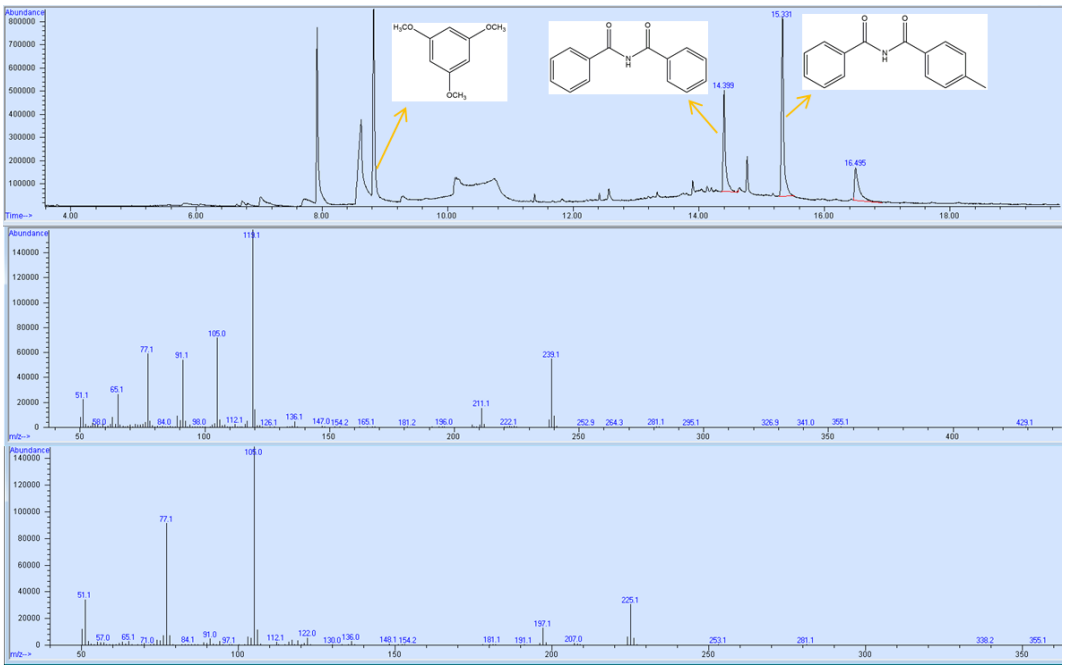

Figure S38. GC-MS data of reaction solution for the (0.045 mmol) reacts with mixture of benzoyl chloride (0.06 mmol) and p-toluoyl chloride (0.12 mmol) with mole ratio of 1:2 after drying treatment of molecular sieve for 24 hours. Theoretical m/z of N-benzoyl-4-methylbenzamide: 239.1; experimental m/z of N-benzoyl-4-methylbenzamide: 239.1. The yield is calculated as 67% based on the amount (30 μmol) of 4-methyl-N-(4-methylbenzoyl)benzamide calculated from its ratio of integral peak area relative to signal peak of N-benzoylbenzamide in the GC-MS chromatogram. The yield of N-benzoylbenzamide calculated from its ratio of integral peak area relative to single ion (m/z = 168.1) signal peak of internal standard (1,3,5-trimethoxybenzene) in the GC-MS chromatogram.

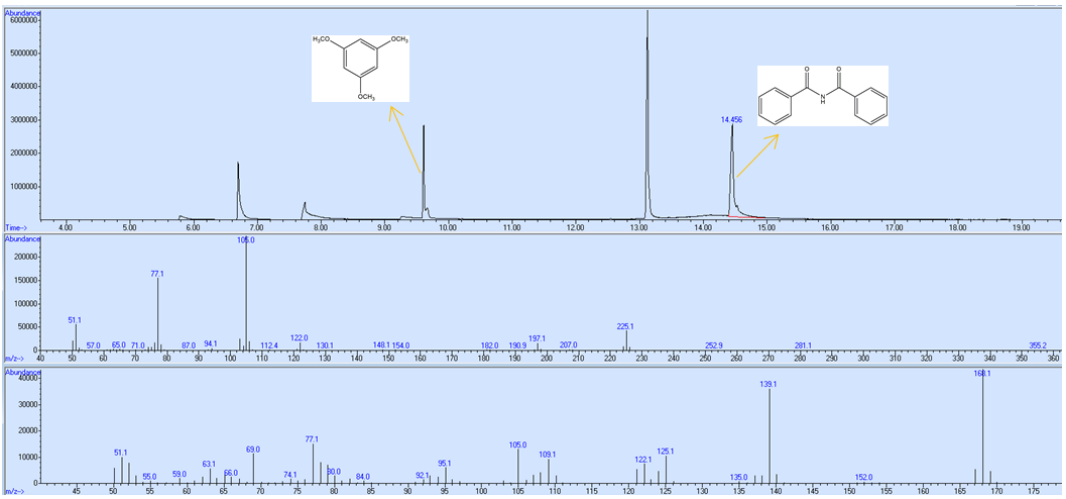

Figure S39. GC-MS data of reaction mixture solution obtained by mixing Li_3N-loaded electrode with benzoyl chloride (0.24 mmol). Theoretical m/z of **2a** N-benzoylbenzamide: 225.1; experimental m/z of **2a** N-benzoylbenzamide: 225.1. The FE is calculated as 73% based on the amount (60.5 μmol) of N-benzoylbenzamide calculated from its ratio of integral peak area relative to single ion (m/z = 168.1) signal peak of internal standard (1,3,5-trimethoxybenzene) in the GC-MS chromatogram. Electrode was prepared from the small two-electrode cells with a current density of –2.5 mA cm^{-2} for 160 min. According to the amount of Li_3N quantified by the indophenol blue method, the yield of N-benzoylbenzamide is 86%, being close to the yield (88%) of controlled experiment using commercially available Li_3N. The result indicates that the SEI shows a negligible influence on the subsequent reaction between Li_3N and acylchloride. There might be two reasons for this: i) In our mixed electrolyte systems, a coulombic efficiency of 91.5% for lithium plating was obtained, allowing for the formation of a very thin SEI layer; ii) Compared with the SEI, the highly reactive Li_3N preferentially reacted with acylchloride.

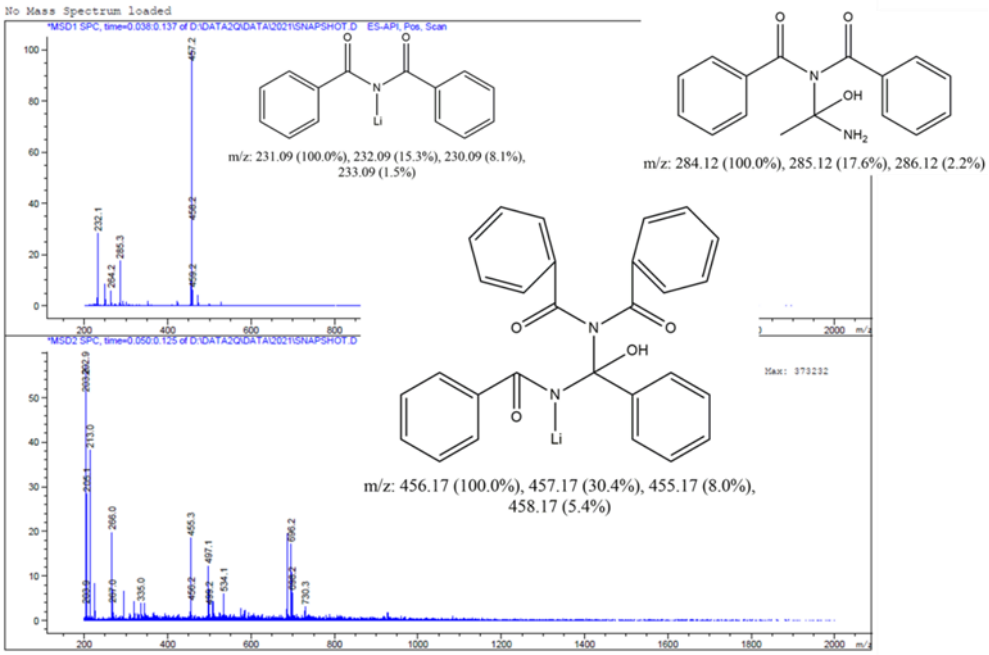

Figure S40. LC-MS data of reaction solution for the Li_3N (0.06 mmol) reacts with two equivalent of benzoyl chloride (0.12 mmol). The signal of 232.1 is assigned to [N-benzoylbenzamide-Li+H]$^+$. Other signals are attributed to the coupling of the N-benzoylbenzamide-Li or N-benzoylbenzamide and solvent during LC-MS measurement. The spectrum was collected using HP-LC grade acetonitrile as solvent.

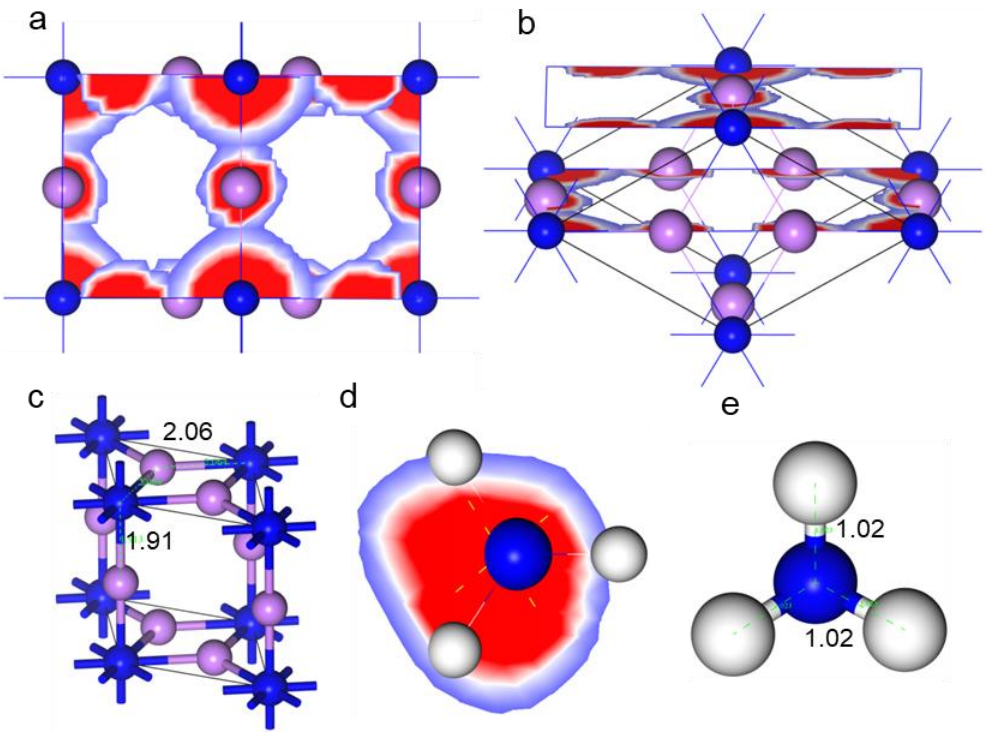

Figure S41. The electron density of (a) top view of Li_3N, (b) side view of Li_3N, and (d) top view of NH_3, suggesting that Li_3N is a chemically reactive compound due to a mutually-exclusive relationship between N atoms and Li atoms. The red electronic cloud indicates electron accumulation and the blue electronic cloud indicates electron depletion. The electron density of Li_3N in the plane of the top lithium atom and central two-dimension layer was cut. (c) Li-N and (e) H-N bond length in Li_3N and NH_3, respectively. White, blue, and purple spheres represent the H, N, and Li atoms, respectively. In the modelling experiments, the charge clouds determining nucleophilicity and crystalline structure of Li_3N (space group P6/mmm, also confirmed by the XRD result in Figure S9) are found responsible for the high selectivity of aryl imides synthesis in heterogeneous fashion. The electron density shows electronic accumulation (red clouds) in both N atoms and Li atoms, being different from usual bond structure (Figure S41a,b), such as N–H bond in NH_3 (Figures S41d,e). The bonding character makes the N-Li bonds longer and the Li_3N highly active (Figure S41c), while providing enough space for the carbonyl carbon to approach the nucleophile (N atom due to its higher electronegativity compared to Li atoms). The Li_3N crystal is a layered structure composed of sequential Li_2N layers and Li.

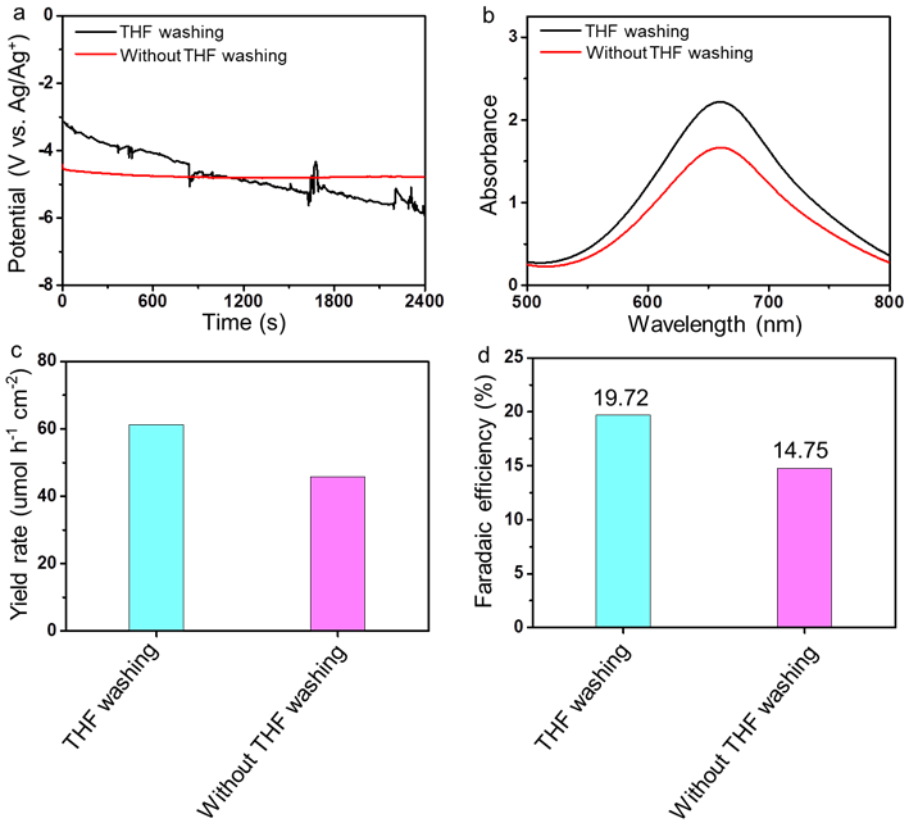

Figure S42. The performance comparison of Li_3N-deposited electrodes with and without washing surface residual PC by immersed in THF for 10 s after electroplating in PC//PC system at a current density of –15 mA cm^{-2}. (**a**) Chronoamperometry curves. (**b**) Corresponding UV-visible absorption spectra for NH_3 measurement after the nitridation and hydrolysis processes. Corresponding (**c**) yield rates and (**d**) Faradaic efficiencies of Li_3N. The results show that the residual PC on the surface will react with Li metal to make the performance reduced.

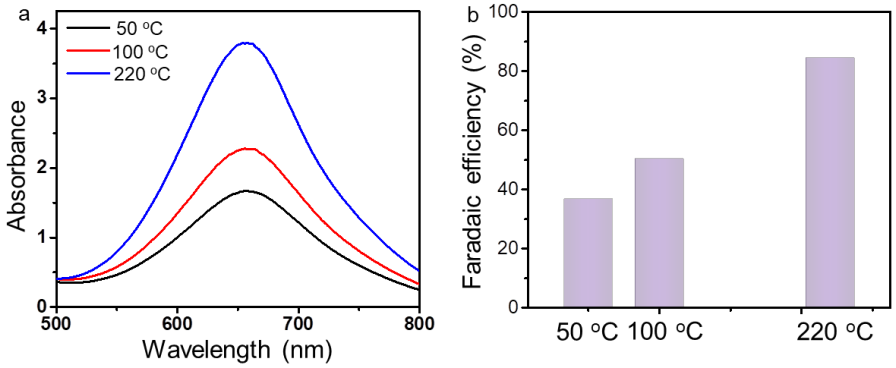

Figure S43. The performance comparison of Li_3N-deposited electrodes for the nitridation process conducted at several temperature levels after electroplating in 1 M $LiPF_6$/EC:DEC:EMC=1:1:1 by volume with 2 wt% VC additive at current of –2.5 mA for 160 min. (**a)** UV-visible absorption spectra for NH_3 measurement after the nitridation and hydrolysis processes. (**b**) Corresponding Faradaic efficiencies of Li_3N. The exposure of deposited Li to N_2 atmosphere was carried out at various temperature for 30 min. Appropriate heating treatment can facilitate a rapid process of Li nitridation when the loading Li metal on the electrode is thick. There are two kind of Li-mediated methods, whose difference is whether the Li plating and nitridation are run simultaneously or with temporal separation. The former is usually run at room temperature, because it only briefly forms a small amount of lithium nitride on the electrode surface that is rapidly protonated to form ammonia.[12,13] However, this method need use alcohols or H_2 as a proton source to avoid rapid hydrolysis of formed Li metal. The later (used in this work) generally need moderate temperature to facilitate the nitridation process due to a thick Li layer loaded on electrode.[14] The advantage of this method is that water can be used as a proton source, and the resulting current efficiency is relatively high. Inspired from the comment, the performance comparison after nitridation at several temperature levels (50, 100, 220 ^oC) were studied (Figure S43), which demonstrate appropriate heating treatment (220 ^oC) can help the Li nitridation proceed quickly.

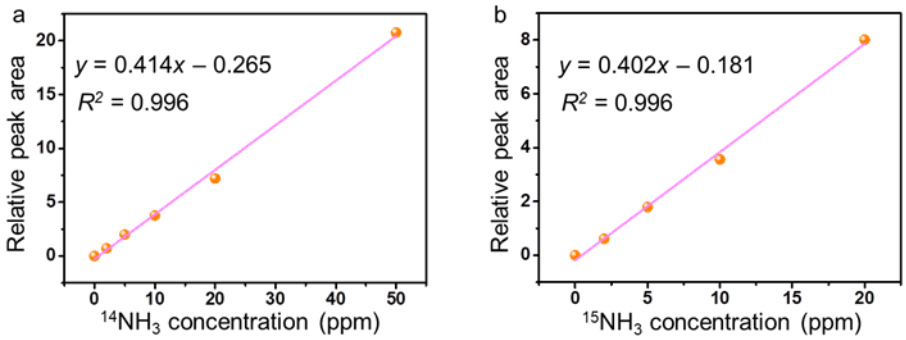

Figure S44. Plotting of standard curves of (**a**) $^{14}NH_3$ and (**b**) $^{15}NH_3$ in 0.05 M hydrochloric acid solution. The ammonia was quantified by ^{1}H NMR measurement. The spectra were collected in D_2O with maleic acid as internal standard.

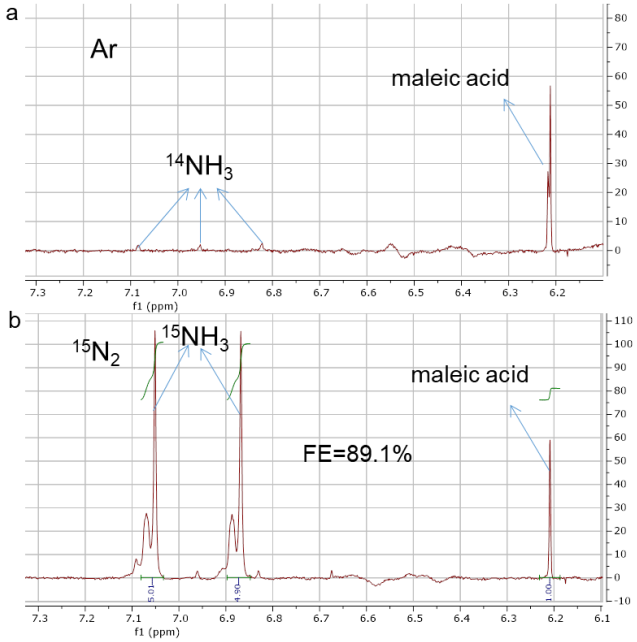

Figure S45. Control experiments for the nitridation process with Li-deposited electrode exposed at Ar and $^{15}N_2$ atmospheres. ^{1}H NMR spectra for NH_3 measurement after the nitridation and hydrolysis processes at (**a**) Ar and (**b**) $^{15}N_2$ atmospheres. The spectra were collected in D_2O with maleic acid as internal standard. Electrodes were prepared from the small two-electrode cells with a current density of –2.5 mA cm^{-2} for 160 min. The ^{15}N labeled nitride was synthesized with FE of 89.1% when using the $^{15}N_2$ as nitrogen source, demonstrating that the nitrides used in the synthesis reaction were derived from N_2 fixation. Under Ar environment, negligible nitride was produced. It should be noted that the splitting of typical $^{15}NH_4^+$ doublet into a quartet is because $^{15}NH_4^+$ in aqueous has two chemical environments. The strong signal represents the $^{15}NH_4Cl$, and the weak signal represents $^{15}NH_3 \cdot H_2O$.

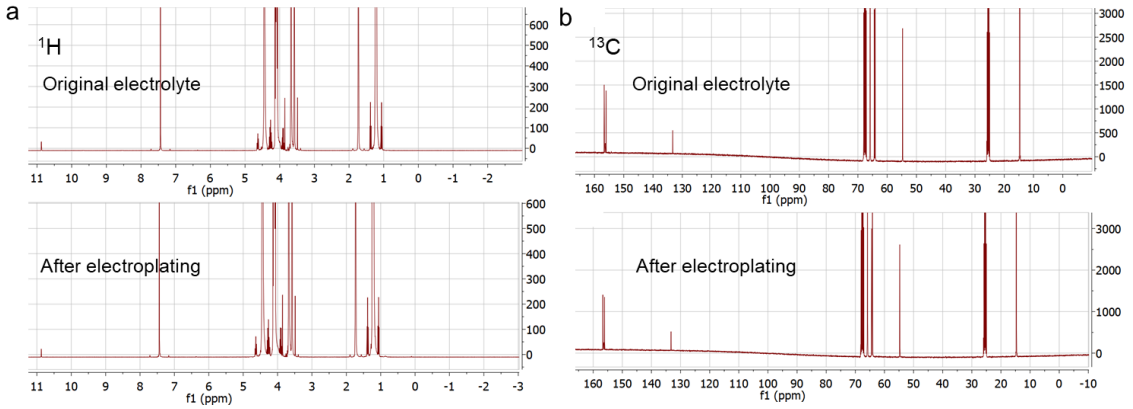

Figure S46. (**a**) The ^{1}H and (**b**) ^{13}C NMR of electrolyte before and after the electroplating, showing the electrolyte was basically unchanged after used for electroplating and indicating the electrolyte is able to stand the test of constant operation. The spectra were collected in THF-d_8.

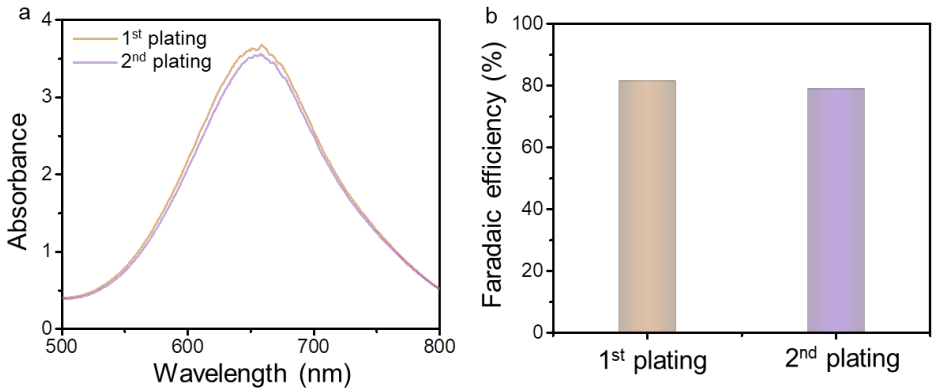

Figure S47. Electrolyte reused experiment by electroplating twice in same electrolyte with only changing the electrodes. Electroplating experiments were conducted in battery with electrolyte of 1 M $LiPF_6$/EC:DEC:EMC=1:1:1 by volume (containing 2 wt% VC additive) at current of –2.5 mA for 160 min. (**a)** UV-visible absorption spectra for NH_3 measurement after the nitridation and hydrolysis processes. (**b**) Corresponding Faradaic efficiencies of Li_3N.

III. Supporting Tables

Table S1. Compilation of literature reported Faradaic efficiency in Li-mediated N_2 fixation.

Electrode	Electrolyte	Conditions	Faradaic efficiency	Potential/Voltage (Current)
Copper foil[10]	1 M $LiBF_4$, 0.2 M EtOH, THF	Ambient	18.5%	15 V (8 mA cm^{-2})
Silver foil[11]	0.2 M $LiClO_4$, 0.18 M EtOH, THF	Ambient	8.4%	>-4 V vs. Ag/AgCl (2 mA cm^{-2})
Iron foil[12]	0.2 M $LiClO_4$, 0.18 M EtOH, THF	50 bar N_2, 25 ℃	57.7%	>-4 V vs. Ag/AgCl (2 mA cm^{-2})
Molybdenum foil[12]	0.2 M $LiClO_4$, 0.18 M EtOH, THF	Ambient	7.5%	9 V (2~3 mA)
Stainless steel cloth, GDE[13]	1 M $LiBF_4$, 0.1 M EtOH	Ambient	35.5%	30.2 V(25 mA cm^{-2})
nickel foil[14]	1 M $LiClO_4$/PC	220 ^oC	49.9%	6.2~6.8 V (5 mA cm^{-2})
Mo foil[15]	0.3 M $LiClO_4$, 1% vol. EtOH, 99% vol. THF	10 bar N_2, 25 ℃	37.1%	1 V vs. Li/Li^+ (−2 mA cm^{-2})
Cu foil (This work)	0.2 M LiCl/THF:PC = 1:1 by vol.	220 ^oC	76.7%	<-0.2 V vs. Li/Li^+ (−0.5 mA)
Cu foil (This work)	1 M $LiPF_6$/ EC:DEC:EMC = 1:1:1 by vol.	220 ^oC	84.6%	-0.25 V vs. Li/Li^+ (−2.5 mA)

IV. Supplementary Notes

Supplementary Note 1.

To verify the feasibility to synthesize arylimides from Li_3N and acid chlorides, first we attempted to react Li_3N with different equivalents of benzoyl chloride. Interestingly, no matter how many equivalents of benzoyl chloride were used, the reaction always produced dibenzamide **2a** (N-benzoylbenzamide) (Figures S29-S31). A high yield of 88 % was achieved using two equivalents of benzoyl chloride (Figures 4d and S32). A small amount of benzamide **1a** was also detected in the GC-MS, which should be ascribed to the reaction of NH_3 from the acidolysis of a small amount of Li_3N with benzoyl chloride.

Supplementary Note 2.

To demonstrate the method in this work has great advantages from the overall energy efficiency, economic benefits, and significance of the reaction points of view, the reaction conditions among using Li_3N for imides synthesis, hydrolyzing Li_3N to NH_3, and using NH_3/amines for imides synthesis are compared and discussed, as following:

On the face of it, the reaction conditions of hydrolyzing Li_3N to NH_3 is indeed simpler than that using Li_3N for imides synthesis. However, considering that the generated NH_3 still needs to be separated and purified for the subsequent reaction, the direct reaction of Li_3N-loaded electrodes without purification appear to be very advantageous.

Actually, for most imides synthesis using Li_3N, commercially available reagents can be used directly for the reaction. For example, the synthesis of more common imides, such as N-benzoylbenzamide and isoindoline-1,3-dione, commercially available THF (Sigma-Aldrich, anhydrous, ⩾99.9%, inhibitor-free), benzoyl chloride (Sigma-Aldrich, 99%) and o-phthaloyl chloride (Sigma-Aldrich, 90%) can be used directly. Some of commercial acid chlorides may contain a lot of carboxylic acid and HCl impurities derived from hydrolysis of acid chlorides. In this case, the Li_3N will react with HCl instead of acid chloride. In order to improve the yield, phenylacetyl chloride and p-toluoyl chloride did require additional step of treatment with molecular sieves to remove impurities before using for the reactions. But these acid chlorides, even if it does not use Li_3N as the reactant, use ammonia or amines as the reactant, should better be pretreated first to improve the yield. In addition, the treatment process by molecular sieves is very simple and common in synthesis industry, and recovery of molecular sieves is a straightforward procedure.

More importantly, using Li_3N can not only reduce energy loss, it can also improve the synthesis efficiency of imides, which traditionally requires two steps to complete the reaction, but with Li_3N can be completed in one step. In addition, the yield of the traditional method is very low. Only 9% for the amidation reaction of the benzamide and benzoyl chloride (12% reported in literature)[16]. While the yield of that using lithium nitride can reach 67~91%. Therefore, the method in this work has great advantages from the overall energy efficiency, economic benefits, and significance of the reaction.

Supplementary Note 3.

The electrolyte is recyclable for Li_3N synthesis. In the field of lithium batteries, secondary batteries can be cycling charged-discharged hundreds of times. In this work, the lithium is the only consumable. The electrolyte can be reused as long as lithium salt is

constantly replenished. To prove this, we conducted two experiments to illustrate. (i) The ^{1}H and ^{13}C NMR show basically unchanged components of electrolyte after the electroplating compared to that of the original electrolyte (Figure S46), indicating the electrolyte stands the test of constant operation; (ii) After the first electroplating, we replaced the lithium-loaded Cu foil with a new bare Cu foil for electroplating again. The performance (FE=79.1%) of secondary Li_3N synthesis is close to that (81.7%) of first one (Figure S47).

Supplementary Note 4.

Economic applicability. We take N-benzoylbenzamide as an example to calculate the cost of aryl imides synthesis from commercially available Li_3N with benzoyl chloride by considering the cost of reagents/solvents and compare with that of synthesis from commercially available benzamide with benzoyl chloride. The cost of separation and purification is not considered here because the product purification procedure of two methods is the same after the reactions. Based on our experiments, we assume 15 mL of solvents are needed to synthesize 1 gram of N-benzoylbenzamide, and according to the yield, the required amounts of reactants can be inferred. Specifically, to synthesize one gram of product, 15 mL THF, 0.18 g Li_3N, and 1.42 g benzoyl chloride are required for the former and 15 mL pyridine, 5.98 g benzamide, and 6.94 g benzoyl chloride are required for the latter. All reagents/solvents cost is based on the price in the Sigma-Aldrich (THF: 0.157 €/mL, pyridine 0.229 €/mL, Li_3N: 6.6 €/g, benzamide: 0.394 €/g, benzoyl chloride: 0.055 €/g). To sum up, 3.56 € is needed to synthesize 1 gram of N-benzoylbenzamide from commercially available Li_3N by taking into account cost of reagents/solvents, while 6.18 €/g is required for the synthesis of N-benzoylbenzamid from commercially available benzamide.

In conclusion, it is economically beneficial to synthesize aryl imides using commercially available Li_3N at current market prices. Of course, this approximate calculation is only in the case of small amounts of synthesis. It would be cheaper when they are produced on larger scale (kg-ton scale), while the cost of reagents in such case is much lower than the price per 1-100 g typically available at Sigma-Aldrich.

Supporting References

[1] B. Delley, *J. Chem. Phys.* **1990**, *92*, 508–517.

[2] B. Delley, *J. Chem. Phys.* **2000**, *113*, 7756–7764.

[3] J. P. Perdew, K. Burke, M. Ernzerhof, *Phys. Rev. Lett.* **1996**, *77*, 3865–3868.

[4] S. Grimme, *J. Comput. Chem.* **2006**, *27*, 1787–1799.

[5] H. Li, Y. Wu, C. Li, Y. Gong, L. Niu, X. Liu, Q. Jiang, C. Sun, S. Xu, *Appl. Catal. B Environ.* **2019**, *251*, 305-312.

[6] A. Trowbridge, D. Reich, M. J. Gaunt, *Nature* **2018**, *561*, 522–527.

[7] L. Wang, A. Menakath, F. Han, Y. Wang, P. Y. Zavalij, K. J. Gaskell, O. Borodin, D. Iuga, S. P. Brown, C. Wang, K. Xu, B. W. Eichhorn, *Nat. Chem.* **2019**, *11*, 789–796.

[8] S.-H. Kang, D. Abraham, A. Xiao, B. Lucht, *J. Power Sources* **2008**, *175*, 526–532.

[9] K. Kanamura, H. Tamura, S. Shiraishi, Z. I. Takehara, *J. Electrochem. Soc.* **1995**, *142*, 340.

[10] N. Lazouski, Z. J. Schiffer, K. Williams, K. Manthiram, *Joule* **2019**, *3*, 1127–1139.

[11] A. Tsuneto, A. Kudo, T. Sakata, *J. Electroanal. Chem.* **1994**, *367*, 183–188.

[12] S. Z. Andersen, V. Čolić, S. Yang, J. A. Schwalbe, A. C. Nielander, J. M. McEnaney, K. Enemark-Rasmussen, J. G. Baker, A. R. Singh, B. A. Rohr, M. J. Statt, S. J. Blair, S. Mezzavilla, J. Kibsgaard, P. C. K. Vesborg, M. Cargnello, S. F. Bent, T. F. Jaramillo, I. E. L. Stephens, J. K. Nørskov, I. Chorkendorff, *Nature* **2019**, *570*, 504–508.

[13] N. Lazouski, M. Chung, K. Williams, M. L. Gala, K. Manthiram, *Nat. Catal*. **2020**, *3*, 463–469.

[14] K. Kim, S. J. Lee, D. Y. Kim, C. Y. Yoo, J. W. Choi, J. N. Kim, Y. Woo, H. C. Yoon, J. I. Han, *ChemSusChem* **2018**, *11*, 120–124.

[15] S. Z. Andersen, M. J. Statt, V. J. Bukas, S. G. Shapel, J. B. Pedersen, K. Krempl, M. Saccoccio, D. Chakraborty, J. Kibsgaard, P. C. K. Vesborg, J. Nørskov, I.,Chorkendorff, *Energy Environ. Sci.* **2020**, *13*, 4291–4300.

[16] A. Trowbridge, D. Reich, M. J. Gaunt, *Nature* **2018**, *561*, 522–527.